N-1810

NCEL

Technical Note

March 1990

By J.S. Bendat, P.A. Palo,
and R.N. Coppolino

Sponsored By Office of
Naval Research

IDENTIFICATION TECHNIQUES FOR NONLINEAR DIFFERENTIAL EQUATIONS OF MOTION

ABSTRACT This report develops and systematically demonstrates by computer simulations new nonlinear system stochastic techniques to determine the amplitude-domain and frequency-domain properties of nonlinear systems as described in proposed nonlinear differential equations of motion. From measurements of input excitation data and output response data, it is shown that this new method, based upon multiple-input/single-output (MI/SO) linear analysis of reverse dynamic systems, allows for the efficient identification of different nonlinear systems. Nonlinear systems simulated here include Duffing, Van der Pol, Mathieu, and Dead-Band systems.

NAVAL CIVIL ENGINEERING LABORATORY PORT HUENEME CALIFORNIA 93043-5003

METRIC CONVERSION FACTORS

Approximate Conversions to Metric Measures

Symbol	When You Know	Multiply by	To Find	Symbol
		LENGTH		
in	inches	*2.5	centimeters	cm
ft	feet	30	centimeters	cm
yd	yards	0.9	meters	m
mi	miles	1.6	kilometers	km
		AREA		
in^2	square inches	6.5	square centimeters	cm^2
ft^2	square feet	0.09	square meters	m^2
yd^2	square yards	0.8	square meters	m^2
mi^2	square miles	2.6	square kilometers	km^2
	acres	0.4	hectares	ha
		MASS (weight)		
oz	ounces	28	grams	g
lb	pounds	0.45	kilograms	kg
	short tons (2,000 lb)	0.9	tonnes	t
		VOLUME		
tsp	teaspoons	5	milliliters	ml
Tbsp	tablespoons	15	milliliters	ml
fl oz	fluid ounces	30	milliliters	ml
c	cups	0.24	liters	l
pt	pints	0.47	liters	l
qt	quarts	0.95	liters	l
gal	gallons	3.8	liters	l
ft^3	cubic feet	0.03	cubic meters	m^3
yd^3	cubic yards	0.76	cubic meters	m^3
		TEMPERATURE (exact)		
°F	Fahrenheit temperature	5/9 (after subtracting 32)	Celsius temperature	°C

*1 in = 2.54 (exactly). For other exact conversions and more detailed tables, see NBS Misc. Publ. 286, Units of Weights and Measures, Price $2.25, SD Catalog No. C13.10:286.

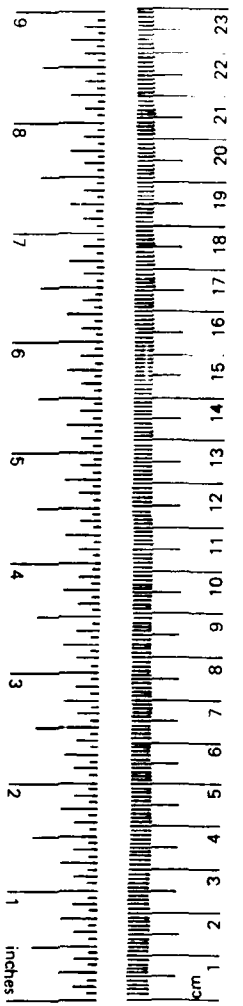

Approximate Conversions from Metric Measures

Symbol	When You Know	Multiply by	To Find	Symbol
		LENGTH		
mm	millimeters	0.04	inches	in
cm	centimeters	0.4	inches	in
m	meters	3.3	feet	ft
m	meters	1.1	yards	yd
km	kilometers	0.6	miles	mi
		AREA		
cm^2	square centimeters	0.16	square inches	in^2
m^2	square meters	1.2	square yards	yd^2
km^2	square kilometers	0.4	square miles	mi^2
ha	hectares (10,000 m^2)	2.5	acres	
		MASS (weight)		
g	grams	0.035	ounces	oz
kg	kilograms	2.2	pounds	lb
t	tonnes (1,000 kg)	1.1	short tons	
		VOLUME		
ml	milliliters	0.03	fluid ounces	fl oz
l	liters	2.1	pints	pt
l	liters	1.06	quarts	qt
l	liters	0.26	gallons	gal
m^3	cubic meters	35	cubic feet	ft^3
m^3	cubic meters	1.3	cubic yards	yd^3
		TEMPERATURE (exact)		
°C	Celsius temperature	9/5 (then add 32)	Fahrenheit temperature	°F

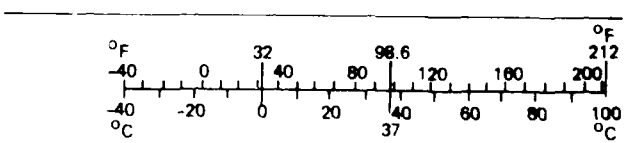

REPORT DOCUMENTATION PAGE

Form Approved
OMB No. 0704-018

1. AGENCY USE ONLY *(Leave blank)*	2. REPORT DATE	3. REPORT TYPE AND DATES COVERED
	March 1990	Final; October 1988 to March 1990

4. TITLE AND SUBTITLE

IDENTIFICATION TECHNIQUES FOR NONLINEAR DIFFERENTIAL EQUATIONS OF MOTION

5. FUNDING NUMBERS

PE - RR000.01.205
WU - DN669036

6. AUTHOR(S)

J. S. Bendat, J.S. Bendat Co.
P.A. Palo, NCEL
R. N. Coppolino, Measurement Analysis Corp.

7. PERFORMING ORGANIZATION NAME(S) AND ADDRESSE(S)

Naval Civil Engineering Laboratory
Port Hueneme, CA 93043-5003

8. PERFORMING ORGANIZATION REPORT NUMBER

TN - 1810

9. SPONSORING/MONITORING AGENCY NAME(S) AND ADDRESSE(S)

Office of Naval Research
800 No. Quincy Street
Arlington, VA 22217-5000

10. SPONSORING/MONITORING AGENCY REPORT NUMBER

11. SUPPLEMENTARY NOTES

12a. DISTRIBUTION/AVAILABILITY STATEMENT

Approved for public release, distribution is unlimited.

12b. DISTRIBUTION CODE

13. ABSTRACT *(Maximum 200 words)*

This report develops and systematically demonstrates by computer simulations new nonlinear system stochastic techniques to determine the amplitude-domain and frequency-domain properties of nonlinear systems as described in proposed nonlinear differential equations of motion. From measurements of input excitation data and output response data, it is shown that this new method, based upon multiple-input/single-output (MI/SO) linear analysis of reverse dynamic systems, allows for the efficient identification of different nonlinear systems. Nonlinear systems simulated here include Duffing, Van der Pol, Mathieu, and Dead-Band systems.

14. SUBJECT TERMS

Systems identification; nonlinear systems; Duffing systems; Van der Pol systems; Mathieu systems

15. NUMBER OF PAGES

58

16. PRICE CODE

17. SECURITY CLASSIFICATION OF REPORT	18. SECURITY CLASSIFICATION OF THIS PAGE	19. SECURITY CLASSIFICATION OF ABSTRACT	20. LIMITATION OF ABSTRACT
Unclassified	Unclassified	Unclassified	UL

CONTENTS

1.0 INTRODUCTION

1.1 Motivation

A large number of physical dynamic systems are nonlinear; practically all dynamic systems are nonlinear if the excitation is high enough. The behavior of most structures, while subject to extreme excitations, represents the design condition. Therefore, accurate knowledge of their dynamic properties is crucial.

Where does this information come from? For some systems, the dynamic properties can be computed theoretically. In some limited cases, specialized subtests can be conducted and the results combined to approximate the total system behavior. More often, however, the complexity of the nonlinear interactions make it necessary to perform tests on the complete system to determine its behavior. If the analyst is extremely fortunate, there may even be full-scale measurements of excitation(s)/system response(s) directly representing the extreme loading (design) case. A more common situation is to have one set of measurements representing the excitation/responses for a level of excitation variance lower than the design level.

Even when an accurate data set is available, the analyst is only slightly better off than before because nonlinear system theory is not well developed. A "single useful method" for identifying and quantifying nonlinear system properties does not exist. While some techniques do exist and could possibly be applied by an experienced user, the results are limited, expensive, and difficult to interpret.

The U.S. Navy often faces this scenario while designing new prototype systems for which there is no historical basis for design. The development of a general nonlinear system identification procedure has been underway at the Naval Civil Engineering Laboratory (NCEL) since 1980, motivated primarily by the need for an improved understanding of

vessel moorings and dynamic wave loads (Ref 1). Development of the basic frequency-domain mathematical framework used as the foundation of this new method was partially sponsored by NCEL and has been recently published (Ref 2).

This report summarizes the development of a new approach to nonlinear system identification developed through NCEL that has been successfully applied to a variety of simulated nonlinear systems.

1.2 State of the Art in Higher Order System Identification

General nonlinear systems exhibit a more complex behavior than linear systems. Accordingly, much of the research in nonlinear systems theory has been directed toward defining a universally applicable mathematical model capable of simultaneously converting one arbitrary, stationary, input variable into the many terms that comprise the nonlinear output. Such a theory has not yet been discovered.

The nonlinear formulation with the most universal application is the so-called Volterra series (Ref 3). The Volterra series assumes that the nonlinear response can be expanded as a "power series with memory," with an N-integral kernel associated with each nth order component. This approach leads to higher order spectra such as bispectra and trispectra that are based on higher order cumulants of the input time history. Some of the disadvantages of Volterra series are:

(a) Unreasonable computer processing requirements for kernels of order four or more.

(b) Sensitivity to the distribution of the input signal and noise.

(c) Difficulty in interpreting system behavior by inspection of third and higher order kernels.

(d) Large random errors that require excessive (often unobtainable) amounts of data for acceptable confidence limits.

Thus, in practice, the Volterra series is typically applied only when the highest order response is assumed to be second-order or third-order. It is noted that the Volterra kernels are invariant to input excitation levels only when the assumed and physical highest order responses are the same.

Reference 3 provides a very complete overview of the Volterra and related Wiener nonlinear system theories. Reference 4 is a similarly complete review of the theory, computation, and applications of the bispectrum. Autoregressive (AR), Moving Average (MA), or combined (ARMA) models have also been used to describe higher order system responses (Ref 5). However, these models do not provide system parameters appropriate for structural problems. Reference 6 summarizes much of the latest research activity and applications in higher order spectral analysis.

1.3 Problem Description

As stated in Section 1.1, NCEL has had a continual need for nonlinear systems identification techniques. Some specific examples include:

(a) Wave-induced forces on slender members (the Morison equation).

(b) Nonlinear stiffness: catenary (mooring lines), fenders (pierside).

(c) Second-order wave drift forces on ships (proportional to the wave envelope).

(d) Extreme vessel motions.

(e) Buoy motions (nonlinear buoyancy for floating versus submerged).

(f) Time-varying stiffness: fishtailing in single point moorings,

(g) Time-varying mass and stiffness: bottom interaction of mooring lines.

For a nonlinear system like a moored ship, the above-mentioned matters may occur simultaneously. In this case, if a full-scale data set is available, it typically consists of measurements of the inputs consisting of the incident wave and wind vectors, and the system responses of interest, usually consisting of the six vessel motions and selected tensions in the mooring lines (Ref 7). For slender member wave force data sets, the input might consist of either the incident waves or wave velocities while the output is the horizontal component of force in line with the direction of wave advance. For the finite duration of the data set, it is usually assumed that the input data are stationary with constant variance.

In all cases, the purpose for collecting data is to allow for validation of a postulated engineering model of the system. Usually, this model consists of component terms such as: inertial forces; linear and viscous damping forces; restoring forces that represent the equation of motion of the system; and component terms representing the excitation forces (for example, first- and second-order hydrodynamic loads). The validation seeks to identify the nature of the physical process (qualitative properties) and the associated numerical parameters (quantitative properties).

1.4 Overview of Present Study

The objective of the present study was to develop a general nonlinear system identification methodology to determine from measured input and output stochastic data the validity of each term in a proposed nonlinear differential equation of motion. This report describes some of the results obtained by a new practical frequency-domain approach that has been under investigation at NCEL since 1980 (Ref 2 and 8), where established multiple-input/single-output linear procedures are

applied to reverse dynamic systems. Material in this report focuses on single degree-of-freedom (SDOF) nonlinear systems excited by stationary random data; this excitation can be Gaussian or non-Gaussian with arbitrary spectral shape. The new approach is theoretically outlined here and applied to a variety of nonlinear systems.

It is noted that this approach was also used independently in References 9 and 10 based on ideas in Reference 8. This report greatly extends the understanding and application of the material contained in References 8 to 10. It is demonstrated here that this new NCEL-developed method identifies desired nonlinear system properties independent of the probablility or spectral nature of the measured input and output data, excitations levels, or typical extraneous noise levels. Simulated SDOF nonlinear systems include Duffing, Van der Pol, Mathieu, and Dead-Band systems.

2.0 SINGLE DEGREE-OF-FREEDOM (SDOF) NONLINEAR SYSTEMS

2.1 System Descriptions

A broad class of nonlinear SDOF dynamic systems is described by the constant coefficient differential equation:

$$m\ddot{u} + c\dot{u} + ku + p(u,\dot{u},t) = F(t) \tag{2.1}$$

For the mechanical systems addressed in this study, m is the system mass, k is the linear elastic stiffness constant, c is the linear viscous damping, and $p(u,\dot{u},t)$ represents a general nonlinear damping-restoring force function component. The external applied force is F(t) and the displacement response is u(t) or simply u. From a mechanical schematic viewpoint, as described in Figure 1, the above differential equation represents dynamic equilibrium following the relationship:

$$F_r(u,\dot{u},t) = F(t) - m\ddot{u} \tag{2.2}$$

where the total restoring force is

$$F_r(u,\dot{u},t) = c\dot{u} + ku + p(u,\dot{u},t) \tag{2.3}$$

The basic linear case occurs when $p(u,\dot{u},t)$ is zero.

A variety of nonlinear SDOF systems are considered in this paper. They were selected to represent different nonlinear behavior as described by the following nonlinear force components:

(a) Duffing system (Ref 11):

$$p(u,\dot{u},t) = k_3 u^3 \tag{2.4}$$

(b) Van der Pol system (Ref 11):

$$p(u,\dot{u},t) = \frac{c_3}{3}\left(\frac{d}{dt}\right)[u^3] \tag{2.5}$$

(c) Combined Duffing - Van der Pol system:

$$p(u,\dot{u},t) = \left[k_3 + \left(\frac{c_3}{3}\right)\frac{d}{dt}\right] u^3 \qquad (2.6)$$

(d) Mathieu system (Ref 11):

$$p(u,\dot{u},t) = k_m \cos(2\pi f_m + \phi_m)\, u \qquad (2.7)$$

(e) Dead-Band system:

$$p(u,\dot{u},t) = \begin{cases} -ku, & \text{for } |u| \le u_g \\ -ku_g \operatorname{sgn}(u) & \text{for } |u| > u_g \end{cases} \qquad (2.8)$$

(f) Extreme Duffing - Van der Pol system:

Case (c) above, with linear coefficients c = k = 0.

All of the above types of nonlinearity, except for the Mathieu type, describe systems whose characteristics are nonlinear with amplitude. The Mathieu "nonlinearity" in actuality describes a linear system with a periodic, time-dependent stiffness. The nonlinearity for the Dead-Band system is defined so that the effective system stiffness [ku + p(u,$\dot{u}$,t)] is zero for $|u| \le u_g$ and $k[u - u_g \operatorname{sgn}(u)]$ for $|u| > u_g$.

2.2 Simulation of Measured Dynamic Response

When a nonlinear dynamic system model is subjected to a general time-dependent excitation F(t), the dynamic response history, u(t), is normally determined by numerical integration. For the present study, the Adams-Bashforth predictor-corrector method (Ref 12) is employed.

The excitation force F(t) used in all cases is broad band random data following a Gaussian probability distribution. The random force history is formed using a random number generator provided in the MATLAB 386 computer code (Ref 13). The discretization time Δt is 0.02 seconds, which defines the Nyquist cut-off frequency at 25 Hz. A low-pass filter is applied to the raw excitation history to form an applied force history with a nearly uniform spectral content below 12.5 Hz. A record length of 8,192 samples was used in all simulations.

Dynamic properties for all simulated systems were limited to the lower frequency range (below 10 Hz). This choice was made to assure that the numerical simulations using a 0.02-second time increment would be relatively error free.

For situations considered in this paper where extraneous noise effects are studied, a broad band Gaussian random history, uncorrelated with the excitation, is generated and added to the calculated response u(t). This represents a measured displacement corrupted by noise. The applied force is always assumed to be noise free. Numerical values for the noiseless linear and nonlinear systems in this paper are listed in Table 1 in Section 5.1.

3.0 PRELIMINARY ANALYSIS OF MEASURED DATA

3.1 Objectives and Existing Practice

The objectives of preliminary data analysis for a suspected nonlinear system are:

(a) Recognition that nonlinearity is present (or absent).

(b) Identification of the general class of nonlinearity (to minimize analysis).

(c) Estimation of some key system parameters (in some cases).

A variety of data descriptions may be used to accomplish these objectives consisting of excitation and response probability densities (histograms), excitation and response autospectra, and constructed force/displacement plots.

For the case of a linear system subjected to Gaussian random excitation, both the excitation and response probability densities are theoretically Gaussian. However, if the system is nonlinear, the response probability will deviate from the Gaussian form, often in a manner suggesting the nature of the nonlinearity (Ref 2).

A linear SDOF system that is excited by broad band random data typically exhibits response in a narrow band in the vicinity of the resonant frequency. When nonlinearity is present, the response of the system may contain higher harmonics relative to the resonant frequency band. This effect may be noted in the response autospectrum. In addition, for the case of a Mathieu-type system, it will be shown that the response autospectrum provides an estimate of the periodic stiffness frequency.

3.2 Restoring Force/Displacement Relationships

The construction of force/displacement relationships offers an informative means of uncovering the general nature of a subject dynamic system. Given the measured (or calculated) acceleration response u(t) and applied force F(t), the time history of the SDOF system restoring force $F_r(u,\dot{u},t)$ can be constructed provided the system mass m is known. This calculation follows Equation 2.2. It will be shown in the following discussion that the force/displacement patterns associated with response to random and harmonic excitation have similar characteristics whether the system is linear or nonlinear. These patterns clearly reveal the general nature of the system nonlinearity. Patterns for linear systems are presented first, followed by each of the nonlinear systems described in Section 2.1.

Consider a linear SDOF system with viscous damping undergoing simple harmonic motion (SHM) where:

$$u(t) = U \sin(2\pi f_o t) \tag{3.1}$$

The corresponding restoring force history (see Equation 2.3 with $p(u,\dot{u},t)=0$) is:

$$F_r(u,\dot{u},t) = k\ U \sin(2\pi f_o t) + (2\pi f_o)\ c\ U \cos(2\pi f_o t) \tag{3.2}$$

This pair of functions, when plotted with u(t) as the abscissa and $F_r(u,\dot{u},t)$ as the ordinate, will trace a closed oval as illustrated in Figure 2a. When the same dynamic system is subjected to broad band random excitation, a similar geometric pattern having the same oval envelope is obtained as illustrated in Figure 2b. This similarity between harmonic and random excitation based force/displacement plots occurs since the response of a linear SDOF system is narrow band; the general appearance of the displacement response is that of a fluctuating sinusoid with frequency close to the SDOF natural frequency. The slope of the mean value of F_r at any given value of u corresponds to the linear

stiffness k. In addition, the width of the oval at u=0 indicates the value of $(2\pi f_o)cU$. This pattern description applies to both simple harmonic motion and random motion.

For the nonlinear systems under investigation, the patterns associated with restoring force versus displacement exhibit a property similar to that noted for linear systems. In particular, the closed curve traced by imposing a simple harmonic displacement history on the appropriate restoring force relationship (combining Equations 2.4 to 2.8 with 2.3) produces a characteristic nonlinear "signature." The nonlinear force/displacement pattern, due to broad band random excitation, traces a pattern whose envelope is similar to that associated with the simple harmonic displacement based pattern. Force/displacement patterns corresponding to the example nonlinear systems subjected to both types of excitation (with system properties listed in Table 1) are described below:

(a) The Duffing-type restoring force versus displacement traces an envelope with a mean slope following the stiffness nonlinearity as depicted in Figure 3. The hardening spring behavior expected from the Duffing (cubic) restoring force component is clearly evident.

(b) The Van der Pol-type restoring force versus displacement traces an envelope with a mean slope following a constant linear stiffness. The bulbous envelope at the larger displacement levels, shown in Figure 4, is indicative of the Van der Pol damping nonlinearity.

(c) The combined Duffing-Van der Pol-type restoring force, shown in Figure 5, traces an envelope which exhibits the stiffness and damping nonlinearities in a manner consistent with each of the behaviors described above.

(d) The Mathieu-type restoring force versus displacement pattern, shown in Figure 6, traces a fluctuating envelope which alternates between a low and high value of "linear" stiffness.

(e) The Dead-Band (or Gapping)-type system exhibits a clear envelope of restoring force versus displacement, shown in Figure 7, which enables the investigator to estimate the value of the dead band (in this example, between ± 0.0025). In a later section it will be noted that this preliminary dead-band estimate is required for identification of this type of nonlinear system using the spectral method.

3.3 Further Preliminary Analysis for Mathieu-Type Systems

If a SDOF system is suspected to be of the Mathieu-type on the basis of the restoring force/displacement plot, additional preliminary analysis may be performed to estimate the frequency of the fluctuating stiffness (f_m). It can be demonstrated analytically that the response of such a system to broad band random excitation contains significant components at the "mean" natural frequency $f_n = (1/2\pi)\sqrt{k/m}$, and components at the absolute sum and difference frequencies $|f_n+f_m|$ and $|f_n-f_m|$. This property is clearly illustrated in the displacement response auto-spectrum shown in Figure 8 for a system with $f_n = 3$ Hz and $f_m = 1$ Hz.

Some caution must be taken in the interpretation of displacement response autospectra, especially for cases in which $f_m > f_n$. For example, if $f_n = 3$ Hz and $f_m = 5$ Hz, then significant frequency components will occur near 2, 3, and 8 Hz.

4.0 NONLINEAR SYSTEM IDENTIFICATION TECHNIQUE

4.1 Reverse Dynamic Systems

The spectral analysis technique developed in this paper for identification of SDOF nonlinear systems makes use of a "reverse" dynamic system viewpoint (i.e., a reversal of the input/output roles of excitation and response). The advantage of this approach is noted by examining a nonlinear system the usual (forward) way. The excitation/response diagram is shown in Figure 9 for a general SDOF nonlinear system described by Equation 2.1. The linear frequency response function defined by:

$$H(f) = [k - (2\pi f)^2 m + j\,(2\pi f)c]^{-1} \tag{4.1}$$

relates an "effective" excitation force input $F_e(t)$ versus displacement response output $u(t)$, where the effective force is defined as:

$$F_e(t) = F(t) - p(u,\dot{u},t) \tag{4.2}$$

with $p(u,\dot{u},t)$ as a feedback term and $F(t)$ as the applied external excitation force. Due to the presence of the feedback term, identification of the nonlinear system requires use of an (awkward) iterative approach when the above-noted excitation/response viewpoint is taken.

Consider now the alternative viewpoint in which the displacement response $u(t)$ is considered as the input in Equation 2.1, and the excitation force $F(t)$ required to produce that response is calculated as the output. This reverse dynamic system is shown in Figure 10. The nonlinear SDOF system viewed in this manner is now a multiple-input/single-output (MI/SO) system where the number of multiple inputs depends on the nature of the nonlinearity term $p(u,\dot{u},t)$.

All of the nonlinear system types treated in this paper can be described by the generic reverse dynamic three-input/single-output linear model in Figure 11. The input/output path $A_1(f)$ is simply the reciprocal of the linear frequency response function $H(f)$, namely,

$$A_1(f) = k - (2\pi f)^2 m + j(2\pi f)c \tag{4.3}$$

$$= k\left[1 - \left(\frac{f}{f_n}\right)^2 + j\,2\zeta\left(\frac{f}{f_n}\right)\right]$$

with

$$f_n = \frac{1}{2\pi}\sqrt{k/m} \tag{4.4}$$

and

$$\zeta = \frac{c}{4\pi f_n m} \tag{4.5}$$

The nonlinear paths are modeled using the new frequency domain technique, described in Reference 2, that separates each nonlinearity into separate amplitude and frequency functions. This technique is fully described in the next section.

For each system type in Section 2.1, the nonlinear path functions are described below, where $g_j(u)$ represents a zero-memory (amplitude domain) nonlinear function in Figure 11 and $A_j(f)$ represents the associated linear frequency response function:

(a) Duffing

$$g_2(u)=u^3 \qquad A_2(f)=k_3 \qquad g_3(u)=0 \qquad A_3(f)=0 \tag{4.6}$$

(b) Van der Pol

$$g_2(u)=u^3 \qquad A_2(f)=j(2\pi f)\,\frac{c_3}{3} \qquad g_3(u)=0 \qquad A_3(f)=0 \tag{4.7}$$

(c) Combined Duffing-Van der Pol

$$g_2(u)=u^3 \qquad A_2(f)=k_3 + (2\pi f)\,\frac{c_3}{3} \qquad g_3(u)=0 \qquad A_3(f)=0 \tag{4.8}$$

(d) Mathieu

$$g_2(u)=u\cos(2\pi f_m t) \qquad A_2(f)= k_m\cos(\phi_m) \tag{4.9}$$

$$g_3(u)=u\sin(2\pi f_m t) \qquad A_3(f)=-k_m\sin(\phi_m)$$

(e) Dead-Band

$$g_2(u) = \begin{cases} u & \text{for } |u| \le u_g \\ u_g \operatorname{sgn}(u) & \text{for } |u| > u_g \end{cases} \qquad A_2(f) = -k_1 \qquad (4.10)$$

$$g_3(u) = 0 \qquad A_3(f) = 0$$

By defining the subject nonlinear dynamic systems in terms of Equations 4.3 to 4.10, the unknowns consist of the $A_j(f)$ frequency response functions. The known data are u(t), F(t), and the constructed histories defined by $g_j(u)$.

Using the new spectral analysis technique and reverse dynamics converts the original single-input/single-output (SI/SO) nonlinear problem into an equivalent multiple-input/single-output (MI/SO) linear problem. Conversion of the original, difficult-to-analyze nonlinear problem into an easy-to-analyze linear problem is a significant feature of this technique. The general random data analysis procedures for identification of linear frequency response functions $A_j(f)$ developed in References 14 and 15 are presented next. Note that the g_j functions can represent a wide range of physical nonlinearities beyond the sample cases examined in this report.

4.2 MI/SO Analysis of Reverse Dynamic Systems with Zero-Memory Nonlinearities

The usual SDOF linear system satisfies the linear differential equation of motion:

$$m\ddot{u}(t) + c\dot{u}(t) + ku(t) = F(t) \qquad (4.11)$$

where F(t) = force input

u(t) = displacement output

m = mass of the system

c = linear damping coefficient

k = linear stiffness coefficient

The physical parameters m, c, and k are assumed to be constants. For linear systems, a Gaussian force input produces a Gaussian displacement output.

A SDOF system becomes nonlinear when there are nonlinear stiffness terms and/or nonlinear damping terms. With nonlinear stiffness terms as an example, a typical nonlinear differential equation of motion is:

$$m\ddot{u}(t) + c\dot{u}(t) + ku(t) + k_2u^2(t) + k_3u^3(t) = F(t) \qquad (4.12)$$

where k_2 and k_3 are nonlinear stiffness coefficients for u^2 and u^3, respectively. Here, a Gaussian force input produces a non-Gaussian displacement output.

To apply the nonlinear spectral analysis techniques developed in Reference 2, the roles of F(t) and u(t) are reversed as previously discussed. Equation 4.11 then becomes for the linear case:

$$y(t) = m\ddot{x}(t) + c\dot{x}(t) + kx(t) \qquad (4.13)$$

where x(t) = model input = physical output = displacement u(t)

y(t) = model output = physical input = force F(t)

For cases of nonlinear stiffness terms governed by Equation 4.12, when the roles of F(t) and u(t) are reversed, Equation 4.12 becomes:

$$y(t) = m\ddot{x}(t) + c\dot{x}(t) + kx(t) + k_2x^2(t) + k_3x^3(t) \qquad (4.14)$$

It is not necessary here to assume that the input x(t) is Gaussian; the technique is applicable to arbitrary data.

Fourier transforms of both sides of Equation 4.13 yield the linear frequency domain formula:

$$Y(f) = A_1(f)X_1(f) \qquad (4.15)$$

where $Y(f) = \mathcal{F}\{y(t)\}$ (4.16)

$X_1(f) = \mathcal{F}\{x(t)\}$ (4.17)

$A_1(f) = k - (2\pi f)^2 m + j(2\pi f)c$ (4.18)

Note that $A_1(f)$ is the reciprocal of the usual linear frequency response function $H(f)$ for Equation 4.11 as given in Equation 4.1.

For the nonlinear equation with constant coefficients case of Equation 4.14 (zero-memory nonlinearities), Fourier transforms of both sides yield the nonlinear frequency domain formula:

$$Y(f) = A_1(f)X_1(f) + k_2X_2(f) + k_3X_3(f) \quad (4.19)$$

where $Y(f)$, $X_1(f)$, and $A_1(f)$ are given by Equations 4.16 through 4.18 and where $X_2(f)$ and $X_3(f)$ are the Fourier transforms of $x^2(t)$ and $x^3(t)$ denoted by:

$$X_2(f) = \mathcal{F}\{x^2(t)\} \quad (4.20)$$

$$X_3(f) = \mathcal{F}\{x^3(t)\} \quad (4.21)$$

Equation 4.19 can be displayed as a SI/SO nonlinear model as shown in Figure 12.

Figure 12 can be reconfigured into an equivalent three-input/single-output linear model with correlated inputs $X_1(f)$, $X_2(f)$, and $X_3(f)$ as shown in Figure 13. They produce correlated outputs denoted by $Y_1(f)$, $Y_2(f)$, and $Y_3(f)$.

Practical procedures to identify $A_1(f)$, k_2, and k_3 from measured random data of $x(t)$ and $y(t)$ are developed in References 14 and 15. These procedures show how to replace the given set of correlated inputs with a new set of uncorrelated inputs that are calculated using conditioned spectral density functions. There is no requirement that the input data be Gaussian.

4.3 MI/SO Analysis of Reverse Dynamic Systems with Finite-Memory Nonlinearities

More extensive types of nonlinear stiffness properties can occur in physical problems when the nonlinear terms have finite memory and the system operators A_2 and A_3 become arbitrary functions of frequency representing finite-memory convolutions in the time domain. In these cases, Equation 4.19 takes the more general form:

$$Y(f) = A_1(f)X_1(f) + A_2(f)X_2(f) + A_3(f)X_3(f) + N(f) \qquad (4.22)$$

where N(f) represents extraneous uncorrelated output noise. Figure 13 then becomes Figure 14.

For arbitrary input data x(t), by appropriate processing, Figure 14 can be replaced by the equivalent model of Figure 15 with new uncorrelated inputs $X_1(f)$, $X_{2\cdot 1}(f)$, and $X_{3\cdot 2!}(f)$ passing through new linear systems $L_1(f)$, $L_2(f)$, and $L_3(f)$.

The uncorrelated inputs in Figure 15 can be denoted by the simpler notation $Z_j(f)$ as shown in the figure. These inputs produce uncorrelated outputs denoted by $Y_a(f)$, $Y_b(f)$, and $Y_c(f)$ as also shown.

Relations for Figures 14 and 15 are as follows using the notation in Reference 15 for various conditioned spectral density functions:

$$L_1(f) = G_{1y}(f)/G_{11}(f) \qquad (4.23)$$

$$L_2(f) = G_{2y\cdot 1}(f)/G_{22\cdot 1}(f) \qquad (4.24)$$

$$L_3(f) = G_{3y\cdot 2!}(f)/G_{33\cdot 2!}(f) \qquad (4.25)$$

Also,

$$A_3(f) = L_3(f) \qquad (4.26)$$

$$A_2(f) = L_2(f) - [G_{23\cdot 1}(f)/G_{22\cdot 1}(f)]A_3(f) \qquad (4.27)$$

$$A_1(f) = L_1(f) - [G_{12}(f)/G_{11}(f)]A_2(f) - [G_{13}(f)/G_{11}(f)]A_3(f) \qquad (4.28)$$

The system $L_1(f)$ is the optimum linear system to obtain y(t) from x(t). In general, $A_1(f) \neq L_1(f)$.

4.4 Goodness-of-Fit via Coherence Functions

It is standard practice in the analysis of linear MI/SO systems to calculate various coherence functions to quantify the goodness-of-fit of the chosen stochastic model and the numerical results. This is a vitally important step because it provides an absolute measure of how well each term of the postulated model fits the data over specific regions (i.e., each frequency). This level of information is not readily available in time-domain system identification techniques.

In general, care must be taken when coherence functions are calculated for correlated inputs. In these cases, the recommended practice is to uncorrelate the inputs via conditioning, then compute ordinary coherences which can be inspected individually and summed algebraically to get the goodness-of-fit for the entire model. This was the reason for reconfiguring the problem into the form shown in Figure 15 with uncorrelated inputs $Z_j(f)$ and correspondingly uncorrelated outputs $Y_a(f)$, $Y_b(f)$, and $Y_c(f)$. Further details regarding proper calculation and interpretation of coherence functions follows.

The ordinary coherence function $\gamma^2_{xy}(f)$ states the proportion of the output spectrum $G_{yy}(f)$ that is due to $X_1(f)$ passing through the linear system $L_1(f)$ that gives all the ways $X_1(f)$ can go to the total output Y(f). This quantity is the usual linear coherence function between the input $X_1(f)$ and the output Y(f) as defined by:

$$\gamma^2_{xy}(f) = \gamma^2_{1y}(f) = |G_{1y}(f)|^2 / [G_{xx}(f)\, G_{yy}(f)] \tag{4.29}$$

The partial coherence function $\gamma^2_{2y\cdot 1}(f)$ states the proportion of the conditioned output spectrum $G_{yy\cdot 1}(f)$ that is due to the conditioned input $X_{2\cdot 1}(f)$ passing through only the L_2 system to get the conditioned output $Y_{y\cdot 1}(f)$ defined by:

$$\gamma^2_{2y\cdot 1}(f) = |G_{2y\cdot 1}(f)|^2 / [G_{22\cdot 1}(f)\, G_{yy\cdot 1}(f)] \tag{4.30}$$

The nonlinear coherence function $q^2_{xy_b}(f)$ from Reference 2 states the proportion of the total output spectrum $G_{yy}(f)$, not $G_{yy\cdot 1}(f)$, that is due to the conditioned input $X_{2\cdot 1}(f)$ passing through only the L_2 system to go to the total output $Y(f)$, not $Y_{y\cdot 1}(f)$. This is defined by:

$$q^2_{xy_b}(f) = |G_{2y\cdot 1}(f)|^2 / [G_{22\cdot 1}(f)\ G_{yy}(f)] \tag{4.31}$$

But

$$G_{yy\cdot 1}(f) = [1 - \gamma^2_{1y}(f)]\ G_{yy}(f) \tag{4.32}$$

Hence

$$q^2_{xy_b}(f) = [1 - \gamma^2_{1y}(f)]\ \gamma^2_{2y\cdot 1}(f) \tag{4.33}$$

The next partial coherence function $\gamma^2_{3y\cdot 2!}(f)$ states the proportion of the conditioned output spectrum $G_{yy\cdot 2!}(f)$ that is due to the conditioned input $X_{3\cdot 2!}(f)$ passing through the L_3 system to get to the conditioned output $Y_{y\cdot 2!}(f)$, defined by:

$$\gamma^2_{3y\cdot 2!}(f) = |G_{3y\cdot 2!}(f)|^2 / [G_{33\cdot 2!}(f)\ G_{yy\cdot 2!}(f)] \tag{4.34}$$

The nonlinear coherence function $q^2_{xy_c}(f)$ in Reference 2 states the proportion of the total output spectrum $G_{yy}(f)$, not $G_{yy\cdot 2!}(f)$, that is due to the conditioned input $X_{3\cdot 2!}(f)$ passing through only the L_3 system to get to the total output $Y(f)$, not $Y_{y\cdot 2!}(f)$. This is defined by:

$$q^2_{xy_c}(f) = |G_{3y\cdot 2!}(f)|^2 / [G_{33\cdot 2!}(f)\ G_{yy}(f)] \tag{4.35}$$

But

$$G_{yy\cdot 2!}(f) = \left[1 - \gamma^2_{2y\cdot 1}(f)\right] G_{yy\cdot 1}(f)$$

$$= \left[1 - \gamma^2_{2y\cdot 1}(f)\right] \left[1 - \gamma^2_{1y}(f)\right] G_{yy}(f) \qquad (4.36)$$

Hence,

$$q^2_{xy_c}(f) = \left[1 - \gamma^2_{2y\cdot 1}(f)\right] \left[1 - \gamma^2_{1y}(f)\right] \gamma^2_{3y\cdot 2!}(f) \qquad (4.37)$$

With these component coherence functions defined, the summed coherence function for the entire model can be constructed. Using Reference 2, this is defined as the multiple coherence function and is given for this three-input nonlinear model as:

$$\gamma^2_{y:x}(f) = \gamma^2_{xy}(f) + q^2_{xy_b}(f) + q^2_{xy_c}(f) \qquad (4.38)$$

In References 14 and 15 the multiple coherence function for a three-input/single output linear model is:

$$\gamma^2_{y:x}(f) = 1 - \left[1 - \gamma^2_{1y}(f)\right] \left[1 - \gamma^2_{2y\cdot 1}(f)\right] \left[1 - \gamma^2_{3y\cdot 2!}(f)\right] \qquad (4.39)$$

The equivalence of these latter two equations is straightforward to verify.

The linear coherence function $\gamma^2_{xy}(f)$ in Figure 15 is the ordinary coherence function between the input $Z_1(f) = X_1(f)$ and the total output $Y(f)$, denoted by:

$$\gamma^2_{xy}(f) = \gamma^2_{z_1y}(f) \qquad (4.40)$$

The nonlinear coherence function $q^2_{xy_b}(f)$ in Figure 15 can be interpreted as the ordinary coherence function between the input $Z_2(f) = X_{2\cdot 1}(f)$ and the total output $Y(f)$, denoted by:

$$q^2_{xy_b}(f) = \gamma^2_{z_2y}(f) \qquad (4.41)$$

Similarly, the nonlinear coherence function $q^2_{\breve{y}y_c}(f)$ in Figure 15 can be interpreted as the ordinary coherence function between the input $Z_3(f) = X_{3\cdot 2!}(f)$ and the total output $Y(f)$, denoted by:

$$q^2_{xy_c}(f) = \gamma^2_{z_3y}(f) \tag{4.42}$$

Thus, the multiple coherence function for Equation 4.38 can be written as:

$$\gamma^2_{y:x}(f) = \gamma^2_{z_1y}(f) + \gamma^2_{z_2y}(f) + \gamma^2_{z_3y}(f) \tag{4.43}$$

This multiple coherence function includes all terms and reflects the goodness-of-fit of the postulated model at each frequency. A cumulative coherence function, defined as various partial sums of these component coherences for a select number of terms, is presented in the next section. This cumulative coherence allows for inspection of the model for select combinations of terms.

Good models will be obtained at desired frequencies when the multiple or cumulative coherence function is close to unity. The uncorrelated output noise spectrum $G_{nn}(f)$ representing all possible deviations from the postulated model is given by the formula:

$$G_{nn}(f) = [1 - \gamma^2_{y:x}(f)]\, G_{yy}(f) \tag{4.44}$$

The nonlinear coherence function $q^2_{xy_b}$ should <u>not</u> be interpreted as the ordinary coherence function between the input $X(f)$ and the output $Y_b(f)$. In fact, for Gaussian data $x(t)$, the ordinary coherence function between $X(f)$ and $Y_b(f)$ will be zero. Similarly, the nonlinear coherence function $q^2_{xy_c}(f)$ should not be interpreted as the ordinary coherence function between the input $X(f)$ and the output $Y_c(f)$. Again, for Gaussian input data, this ordinary coherence function is also zero.

4.5 Review of Reverse Dynamic System MI/SO Analysis Technique

Summarizing to this point, the original nonlinear system identification problem has been handled as follows:

(a) Perform preliminary analyses to detect the most probable nonlinearities, where the input and output data are reversed.

(b) Postulate a nonlinear differential equation of motion. It is wise at this stage to include higher order terms than expected, for the following reasons:

1) This technique will correctly determine that there is no frequency response function for terms not present in the physical model; calculating this zero-valued function increases confidence that the chosen order of the model accurately represents the physical system.

2) Inclusion of additional terms (e.g., adding k_5 to a Duffing analysis) does not bias the other results; in other words, this technique is not model-dependent.

3) The only cost for this extra information is slightly increased computer analysis costs proportional to the number of extra input paths.

(c) Precompute a time series for each zero-memory nonlinear function $g_j(u)$.

(d) Compute by the MI/SO procedures the various required spectra for solving the uncorrelated form of the model as shown in Figure 15.

(e) Compute conditioned frequency response functions L_j and unconditioned frequency response functions A_j. Pertinent equations are summarized below; the frequency dependence of all functions has been deleted for clarity.

$$L_1 = G_{z_1 y}/G_{z_1 z_1} \tag{4.45}$$

$$L_2 = G_{z_2 y}/G_{z_2 z_2} \tag{4.46}$$

$$L_3 = G_{z_3 y}/G_{z_3 z_3} \tag{4.47}$$

Equations 4.26 through 4.28 relate these L_j functions to the A_j functions.

(f) Compute component and total spectral functions given by:

$$G_{y_a y_a} = |L_1|^2 G_{z_1 z_1} \tag{4.48}$$

$$G_{y_b y_b} = |L_2|^2 G_{z_2 z_2} \tag{4.49}$$

$$G_{y_c y_c} = |L_3|^2 G_{z_3 z_3} \tag{4.50}$$

$$G_{yy} = G_{y_a y_a} + G_{y_b y_b} + G_{y_c y_c} + G_{nn} \tag{4.51}$$

(g) Compute linear and nonlinear coherence functions given by:

$$\gamma^2_{xy} = \frac{G_{y_a y_a}}{G_{yy}} = \frac{|G_{z_1 y}|^2}{G_{z_1 z_1} G_{yy}} \tag{4.52}$$

$$q^2_{xy_b} = \frac{G_{y_b y_b}}{G_{yy}} = \frac{|G_{z_2 y}|^2}{G_{z_2 z_2} G_{yy}} \tag{4.53}$$

$$q^2_{xy_c} = \frac{G_{y_c y_c}}{G_{yy}} = \frac{|G_{z_3 y}|^2}{G_{z_3 z_3} G_{yy}} \tag{4.54}$$

The last three equations give physical meanings to the three coherence functions. Equation 4.38, the sum of these coherences, is then the multiple coherence function that measures the goodness-of-fit of the entire model.

The reason for calling $q^2_{xy_b}$ and $q^2_{xy_c}$ nonlinear coherence functions is because the output spectrum terms $G_{y_b y_b}$ and $G_{y_c y_c}$ are the result of the original input X(f) going through nonlinear transformations (e.g., squaring and cubing) to provide the correlated inputs X_2 and X_3 in Figures 13 and 14. These, in turn, lead to the uncorrelated inputs Z_2 and Z_3 in Figure 15 from which one calculates the uncorrelated outputs Y_b and Y_c to obtain $G_{y_b y_b}$ and $G_{y_c y_c}$.

The first cumulative coherence function is defined as $\gamma^2_{xy}(f)$. This identifies the proportion of the output spectrum due to x(t) passing through the optimum linear system $L_1(f)$. The second cumulative coherence function is defined by $\gamma^2_{xy}(f) + q^2_{xy_b}(f)$. This identifies the proportion of the output spectrum due to x(t) and $z_2(t)$ passing through $L_1(f)$ and $L_2(f)$. The third cumulative coherence function defined by $\gamma^2_{xy}(f) + q^2_{xy_b}(f) + q^2_{xy_c}(f)$ is the same here as the multiple coherence function.

5.0 NUMERICAL RESULTS OF REVERSE DYNAMIC SYSTEM MI/SO ANALYSIS

5.1 Overview

An evaluation of the MI/SO method applied to reverse nonlinear dynamic systems has been conducted for the SDOF systems described in Section 2. The evaluation is presented here in three sections, namely:

(a) All systems excited by a random force with unit variance, without corruption due to noise, to demonstrate applicability of the method.

(b) The Duffing-Van der Pol system excited by various levels of RMS excitation, without corruption due to noise, to verify if the results are independent of excitation energy.

(c) The Duffing-Van der Pol system excited by a random force with unit variance corrupted by various levels of noise, to evaluate the effects of extraneous noise.

The parameters used in the numerical simulations are listed in Table 1.

Table 1. Simulated System Parameters*

System Type	k	c	f_n	ζ	Nonlinear Parameters	
Linear	355.3	3.77	3.0	0.10	-	-
Duffing	355.3	3.77	3.0	0.10	$k_3=2 \times 10^7$	$c_3=0$
Van der Pol	355.3	3.77	3.0	0.10	$k_3=0$	$c_3=2 \times 10^6$
Combined D-VdP	355.3	3.77	3.0	0.10	$k_3=2 \times 10^7$	$c_3=2 \times 10^6$
Mathieu	355.3	3.77	3.0	0.10	$k_m=177.7$	$f_m=1.0$
Dead-Band	355.3	1.89	3.0	0.05	$u_g=0.0025$	
Extreme D-VdP	0	0	0	0	$k_3=2 \times 10^7$	$c_3=2 \times 10^6$

*All systems used unit mass m=1.0.

5 2 Identification of Nonlinear Systems

This first series of simulations was selected to demonstrate that the MI/SO method is capable of correctly identifying the linear and nonlinear properties of a wide variety of nonlinear dynamic systems (with constant coefficients). The numerical techniques used in these simulations were described in Sections 2.1 and 2.2. The applied excitation force used in all cases is illustrated in Figures 16 and 17, which includes a time history segment, the force autospectrum, and the force histogram. The total time history excitation and response for each simulation is 8,192 samples (163.84 seconds), with subrecord lengths of 512 for the Fourier transforms (10.24 seconds). Therefore, each spectral and frequency response function is based on 16 averages with a bandwidth resolution of 0.0977 Hz. As is common practice in linear spectral analysis, a Hanning window was used to reduce the effects of leakage; a 256-point overlap was employed to recover information "lost" due to the windowing.

Table 2 cross-lists the graphical results presented in the subsequent sections according to the type of function and type of nonlinear system. This table is presented to allow for quick inspection of the results.

Table 2. Comparison of Linear and Nonlinear Results

System Type	Figure Numbers			
	Reverse Frequency Response Functions:		Cumulative Coherences	Response Histogram
	Linear	Nonlinear		
SDOF Linear	18a, 18b	- -	19	20
Duffing	21a, 21b	22a, 22b	23	24
Van der Pol	25a, 25b	26a, 26b	27	28
Duffing-Van der Pol	29a, 29b	30a, 30b	31	32
Mathieu	33a, 33b	34a, 34b	35	36
Dead-Band	37a, 37b	38a, 38b	39	40
Extreme Duffing-Van der Pol	41a, 41b	42a, 42b	43	

5.2.1 SDOF Linear System. Results are presented first for a SDOF linear system to illustrate the new technique for this familiar system type. The linear reverse dynamic system frequency responses, A_1 magnitude and phase, are presented in Figure 18a and 18b where f_n=3.0 Hz and ζ = 0.10. This function has been calculated by the usual linear SI/SO technique (dashed line) and the new technique (solid line) which assumed a simple Duffing model. As one would expect, there is virtually no difference between results from the two methods since there is no nonlinearity in the system. The cumulative coherence function provided in Figure 19, which is near unity, confirms the fact that the system is linear with no significant noise corruption. The dip in coherence near resonance is due to the well-known effect of leakage. The response histogram provided in Figure 20 exhibits an apparent Gaussian distribution which further confirms the conclusion that the system was linear.

The linear frequency response function A_1 is the reciprocal of the usual SI/SO function H. The SDOF system stiffness, k (exact value = 355.5), is obtained from the asymptotic behavior of A_1 for f $\longrightarrow$ 0. In addition, the natural frequency, f_n (exact value = 3), is estimated based on the local minimum value of A_1. Consequently, the system mass, m, is estimated using $k/(2\pi f_n)^2$. The value of the viscous damping is estimated on the basis of the magnitude of A_1 at $f=f_n$ where $|A_1| = 2\pi f_n c$.

5.2.2 Duffing SDOF Nonlinear System. Results for a Duffing SDOF system with identical linear system parameters as the above linear system, and cubic stiffness $k_3 = 2 \times 10^7$, are presented next. For this analysis, two inputs are required (as discussed in Section 4.1): u(t), and the cubic displacement $u^3(t)$. Estimates of the linear frequency response A_1 magnitude and phase are provided in Figure 21a and 21b. The results (solid curve) correctly identify this function (since they agree with the results in Figure 18a and 18b from the previous section). The SI/SO based frequency response function returns a "best linear fit" that is corrupted by the correlated cubic stiffness parameter; inspection of that function shows that it incorrectly estimates k = 500 (exact=355) and f_n = 3.6 (exact=3). Because it assumes a linear system model, the usual SI/SO results are not capable of correctly identifying parameters

that are invariant with excitation variance; in fact, estimates of k and m are incorrect for all input variances. While this particular SI/SO frequency response function would hold for all realizations with the same variance, it would vary for different excitation levels, and is therefore an invalid model for this system.

The MI/SO method, however, identifies the nonlinear component of the reverse system frequency response, A_2, as shown in Figure 22a and 22b in terms of its real and imaginary parts. This function is correctly identified; the real part is equal to 2×10^7 (as used in the simulations), and the imaginary part is essentially zero. Thus, the MI/SO technique correctly identified this system as a Duffing system. The validity of these results is confirmed through inspection of the cumulative coherence function shown in Figure 23, which is nearly unity over the entire frequency range. Furthermore, Figure 23 shows that approximately 90 percent of the output passes through the strictly linear path given by L_1. The fact that this system description is excitation-invariant is examined in Section 5.3.

The displacement histogram for the Duffing response relative to the unit input variance is provided in Figure 24. The distortion from Gaussian is rather slight, so it would not serve well as a preliminary analysis tool for identification of this type of nonlinearity.

5.2.3 Van der Pol SDOF Nonlinear System. The basic behavior of a Van der Pol SDOF system with linear system parameters identical with the system described in Section 5.2.1 and cubic damping with $c_3 = 2 \times 10^6$ is presently examined. As with the Duffing, two inputs (u and u^3) are used. Estimates of the linear reverse dynamic system frequency response function magnitude and phase are provided in Figure 25a and 25b. The MI/SO estimate of A_1 (solid curve) correctly identifies this function, while the SI/SO estimate (dashed curve) again identifies an effective linear system corrupted by the nonlinear damping component. As with the SI/SO result for the Duffing system, this estimate is not invariant with input variance.

The MI/SO technique correctly identifies the nonlinear component A_2 as shown in Figure 26a and 26b in terms of the real and imaginary components. Given the nonlinear input of u^3, and the fact that the Van der Pol nonlinearity is proportional to the out-of-phase velocity, the

expected frequency response function would have a negligable real component and an imaginary component equal to 2 x 10^6 times ($2\pi f/3$). Inspection of the log scale in Figure 26b shows that the MI/SO estimates are correct.

Quantitative confirmation of the estimates is confirmed via the cumulative coherence function shown in Figure 27. The lower-valued curve indicates that nearly all of the excitation for this system below 2 Hz is associated with the linear path L_1. Above 2 Hz, the contribution from the nonlinear term increases. The validity of the whole model is confirmed since the cumulative coherence is close to unity over all frequencies. The displacement histogram for this response is shown in Figure 28, showing strong deviations from the Gaussian shape expected for a linear system.

5.2.4 Combined Duffing-Van der Pol SDOF Nonlinear System. The linear and nonlinear parameters used here were identical to the previous simulations. Estimates of the linear reverse frequency response functions are shown in Figure 29a and 29b. As expected, the SI/SO estimate is contaminated by the nonlinear paths, while the MI/SO estimate is accurate.

The estimate for the nonlinear reverse frequency response function A_2 is provided in Figure 30a and 30b in terms of the real and imaginary functions. Comparison to the previous Duffing and Van der Pol values shows that the parameters are again properly identified. Inspection of the cumulative coherence shown in Figure 31 confirms this conclusion.

Note that the histogram for the displacement response shown in Figure 32 appears close to Gaussian, even though there are two additional nonlinear paths for this system. Therefore, this would not provide any useful information for evaluating whether the system was linear or not; indeed, it would probably reinforce the erroneous conclusion that the system was linear.

An important point can be made here on the value of the MI/SO method for nonlinear system identification problems. Even though the absolute contribution from the nonlinear terms is small for this particular simulation (as shown by the coherence functions) and the response is therefore nearly linear, the MI/SO technique successfully identified the system as

nonlinear. Thus, the method appears to be a robust tool of great value. Conversely, a standard SI/SO analysis of the coherence function would almost assuredly have concluded that the system behaved in a linear manner; this would clearly lead to erroneous results for higher values of excitation variance.

5.2.5 Mathieu SDOF Nonlinear System. Nonlinear systems described by the Mathieu equation exhibit temporal rather than amplitude-dependent nonlinear behavior; the fishtailing behavior of vessels at a single point mooring is a good example.

The presence of periodic variation in stiffness is first detected by preliminary data analysis as discussed in Sections 3.1 and 3.2. This information is needed to apply the new technique.

Employing the estimate for f_m, three reverse dynamic inputs are computed for the Mathieu analysis as specified in Equation 4.9. The three frequency response functions A_1, A_2, and A_3 are then identified using the new method. For these simulations, the choice of parameters resulted in negligable output from the A_3 system. In an actual Mathieu system, the phase ϕ_m of the time-varying stiffness is unknown (it is directly related to the arbitrary start time for collecting data); hence, both a cosine and sine component are modeled according to Equation 4.9. For these simulations, $\phi_m = 0$ was used, removing the odd component proportional to the sine, and thereby effectively eliminating the A_3 path.

Estimates of the reverse dynamic linear frequency response function, A_1 magnitude and phase, are provided in Figure 33a and 33b. It is noteworthy that the estimate based on the SI/SO technique (dashed curve) is quite erroneous, indicating apparent additional resonant frequencies at the sum and difference frequencies. However, the coherence associated with the SI/SO estimate (not shown here) is quite low, indicating that the model is probably not linear. Once again, the MI/SO linear frequency response function is correct.

The MI/SO estimate for A_2 is shown in Figure 34a and 34b in terms of the real and imaginary parts. The correct values for these functions are seen to be $Re[A_2] = 178$ and $Im[A_2] = 0$ from Table 1 and Equation 4.9; the estimate is excellent over the portion of the frequency range with the predominant energy.

As before, quantitative confirmation is also provided by the cumulative coherence functions shown in Figure 35. First, the cumulative coherence is essentially unity over the whole range, validating the Mathieu model. Second, the linear component of the response that passes through L_1 is rather low, indicating that a strictly linear model would not provide a very useful model for a Mathieu system.

The displacement histogram for the Mathieu response is provided in Figure 36. The somewhat flattened top section is indicative that the response may have some nonlinear contributions.

5.2.6 Dead-Band SDOF Nonlinear System. Some dynamic systems (for example, a loosely-moored ship) only exhibit a stiffness when the response reaches a certain value. The identification and characterization of such systems is explored here.

A SDOF system with a dead-band spring may be crudely modeled as a Duffing system. If MI/SO analysis is performed on dead-band responses with an assumed Duffing model, a cubic stiffness will be identified. Even though the cumulative coherence function associated with this assumed system would show dramatic improvement over the best linear fit, it will never approach unity if the dead band is of the same order of magnitude as the RMS responses. Moreover, the identified Duffing system will not be invariant to the input excitation. It is imperative to correctly identify the system as having a dead band and to incorporate that information into the MI/SO model.

Assume that preliminary data analysis has correctly identified the value of u_g that defines the dead band. A MI/SO model based on Equation 4.10 can then be formulated (with two inputs).

Estimates of the reverse linear frequency response function, A_1 magnitude and phase, are provided in Figure 37a and 37b, where the dashed curve shows the best-fit linear SI/SO estimate and the MI/SO estimate is shown as the solid curve. The SI/SO estimated natural frequency is too low, which is expected since the best linear stiffness averaged over the entire response range will be very low. The MI/SO estimate is correct.

Figure 38a and 38b show the real and imaginary components of A_2. A relatively accurate estimate of the linear stiffness value (-355) is obtained for all frequencies, with a maximum error of 7 percent in the

2- to 3-Hz band. The cumulative coherence functions for the MI/SO estimates are shown in Figure 39. The linear value of approximately 65 percent approaches unity when the nonlinear contribution is added (the somewhat lower coherence near resonance is due to leakage because of low damping in the system). The response histogram is provided in Figure 40, showing markedly non-Gaussian form.

5.2.7 Extreme Duffing-Van der Pol SDOF Nonlinear System. All of the nonlinear systems studied up to this point were constructed by appending nonlinear terms onto the original, linear, differential equation of motion. And, as shown by the various coherence functions presented for each case, the linear contribution typically dominated the total nonlinear response. This is not unexpected for the types of simple nonlinear systems examined. This final simulation was constructed as an extremely nonlinear system to more fully demonstrate the capabilities of the MI/SO technique compared to usual SI/SO procedures. As stated in Section 2.1, this final system consists of the inertial term, with cubic stiffness and damping only (as given by the combined Duffing-Van der Pol system with the linear stiffness and damping terms zeroed out).

Since the system lacks a linear stiffness, the natural frequency (see Equation 4.4) is identically zero. However, for a given level of excitation variance, this cubic stiffness would appear as a linear stiffness to a best-fit linear analysis; thus, a usual SI/SO analysis would erroneously estimate an apparent (but false) natural frequency. In this case, the SI/SO results would lead to serious quantitative errors (the system mass and linear stiffness) as well as qualitative errors (the basic system behavior).

Estimates of the reverse linear frequency response functions, magnitude and phase, are shown in Figure 41a and 41b. The MI/SO estimate (solid curve) correctly identifies the linear system as $-(2\pi f)^2 m$. The SI/SO estimate (dashed curve) is completely wrong for the reasons discussed above. The MI/SO estimate for A_2, shown in Figure 42a and 42b, is correct as seen by comparison to previous cases. The goodness-of-fit of the MI/SO model is confirmed by the cumulative coherence function shown in Figure 43.

5.3 Results from Different Excitation Levels

It was stated in Section 5.1 that the reverse frequency response functions identified using the MI/SO method are globally valid, that is, that the A_j's are independent of the input variance. This is a required characteristic for any valid nonlinear model. Moreover, it was stated that the effective linear system estimates deduced from SI/SO analysis are valid only for the particular excitation level encountered. These statements are verified in this section by simulating the combined Duffing-Van der Pol nonlinear case (see Section 5.2.4) with a range of excitation variances.

For these simulations, the combined system is subjected to an excitation with mean square values of 0.2, 0.5, 1.0, and 2.0 (the unity variance results were previously presented in Section 5.2.4). The frequency response functions A_1 and A_2 and the cumulative coherence functions are provided for these cases as follows:

Input variance:	0.2	0.5	1.0	2.0
Figure Numbers:	44-46	47-49	29-31	50-52

The estimates of A_1, in order of increasing force variance, are shown in Figures 44, 47, 29, and 50, respectively, for the MI/SO (solid curve) and SI/SO (dashed curve) methods. The MI/SO estimate is invariant while the SI/SO estimates erroneously exhibit an increasing apparent resonance (as expected). Note that both estimates are similar for the lowest force level where the nonlinear effects are minimal.

The MI/SO estimates of A_2, again in order of increasing force variance, are shown in Figures 45, 48, 30, and 51. These results are also invariant with force level. The cumulative coherences for all these simulations are shown in Figures 46, 49, 31, and 52. The near-unity values confirm the validity of the results, and in turn, the validity of the MI/SO identification method for these cases.

5.4 Results from Different Extraneous Noise Levels

A practical system identification method must be capable of detecting signals in the presence of noise. The purpose of the simulations in this section is to numerically evaluate the robustness of the MI/SO method to various levels of noise.

Extraneous noise may occur in both input and output measurements. In the case of linear systems subjected to multiple excitations, the noise source is usually assumed at the output (response) signal only. Such a noise type produces random errors and no biasing errors (Ref 15). In order to be consistent with this assumption, the present study assumes a noise source in the reverse dynamic system inputs $u_j(t)$, which correspond physically to the displacement response. This type of noise, which does not pass through the system, theoretically produces random errors only.

For the purpose of investigating the effects of noise contamination, the combined Duffing-Van der Pol system (see Section 5.2.4) was chosen. Noise-free estimates of A_j and the cumulative coherence were presented in Figures 29 through 31. Analyses of this system with mean square noise levels versus displacement response of 5, 10, and 20 percent are presented. The numerical noise was approximately "white" as discussed in Section 2.1.

The frequency response function estimates A_1 and A_2 and cumulative coherences for these cases are provided as follows:

Noise Level (%)	0	5	10	20
Figure Numbers	29-31	53-55	56-58	59-61

Examination of the A_1 estimates indicates that, although random errors increase with noise level, biasing errors are not significant. The A_2 estimates indicate an increasing level of both random and biasing errors, especially in the imaginary component, as the noise level increases. The cumulative coherence functions, while decreasing slightly as the noise increases, still provide a quantitative confirmation that the model is accurately identifying the system properties.

6.0 CONCLUSIONS

This report has addressed the problem of identifying the properties of nonlinear systems from measurements of input and output stochastic data. This new method for nonlinear system identification is based upon multiple-input/single-output linear procedures applied to reverse dynamic systems that are defined for proposed nonlinear differential equations of motion. It is shown that this new method allows for efficient practical identification of a wide variety of nonlinear system behavior.

Conclusions from this investigation regarding the characteristics and [illegible] of this method are:

1. The method converts the original, single-input/single-output nonlinear problem into an equivalent multiple-input/single-output linear problem, thereby allowing for the use of standard linear theory and established computer programs. Nonlinear system amplitude-domain properties are determined separate from nonlinear system frequency-domain properties.

2. The method computes linear frequency response functions for each nonlinear term in the proposed nonlinear differential equation of motion. The relative contributions from each individual term as well as the entire postulated model can be quantitatively assessed through appropriate cumulative coherence functions.

3. The method identifies specific terms as postulated in the proposed nonlinear differential equation of motion. However, since any number of terms can be investigated, enough terms can be included to assure convergence, and the results need not be model-dependent.

4. The method does not require any assumptions regarding the probability distributions or spectral shapes of the input or output data.

5. The model gives results that are independent of the actual input excitation level as required for valid nonlinear models. Also, the results are not sensitive to typical noise levels.

6. The method correctly identifies nonlinear system properties even for low levels of excitation where conventional single-input/ single-output linear analysis would show a high ordinary coherence and erroneously lead to the conclusion that the system is linear. Thus, the new method improves system identification even for nearly-linear systems.

7. Various types of nonlinear system differential equations of motion were examined, including Duffing, Van der Pol, Mathieu, and Dead-Band. All were successfully identified by applying this method to their reverse dynamic systems.

7.0 RECOMMENDATIONS

1. Investigate force excitations with arbitrary spectral shapes (such as the Pierson-Moskowitz wind-wave model) and apply these excitations to various nonlinear systems.

2. Simulate extended SDOF nonlinear systems with more complicated nonlinear restoring and damping forces than those considered here.

3. Study effects of noise in greater detail for cases of noise at both the inputs and outputs of simulated SDOF systems.

4. Develop procedures for analyzing and identifying different terms in MDOF systems and associated MDOF nonlinear differential equations of motion.

5. Demonstrate these procedures by investigating the properties of an actual nonlinear physical system using measured data.

6. Investigate the use of this new method for the nonlinear system identification of nonlinear equations of motion where the coefficients are not necessarily constants.

ACKNOWLEDGMENTS

The nonlinear system research work reported here was performed by Julius S. Bendat of the J. S. Bendat Company and by Robert N. Coppolino of Measurement Analysis Corporation (MAC). Computer simulation studies were made with MAC computers located in Torrance, California. Guidance for this work and material on its need for Navy applications was provided by Paul A. Palo from the Ocean Structures Division at the Naval Civil Engineering Laboratory (NCEL) in Port Hueneme, California.

This investigation was sponsored by NCEL and the Office of Naval Research (ONR). The research was performed through the J.S. Bendat Company under NCEL Contract N62474-86-C-7275.

REFERENCES

1. Naval Civil Engineering Laboratory. Technical Note N-1604: The 1980 CEL mooring dynamics seminar, by P.A. Palo. Port Hueneme, CA, Mar 1981.

2. J.S. Bendat. Nonlinear system analysis and identification from random data. New York, NY, Wiley-Interscience, 1990.

3. M. Schetzen. The Volterra and Wiener theories of nonlinear systems. New York, NY, Wiley-Interscience, 1980.

4. C.L. Nikias, and M.R. Raghuveer. "Bispectrum estimation: A digital signal processing framework," in Proceedings of the Institution of Electrical and Electronics Engineers (IEEE), vol 75, no. 7, Jul 1987.

5. J.M. Mendel. "Use of higher-order statistics in signal processing and system theory: An update," Society of Photo-Optical Instrumentation Engineers (SPIE) Conference on Advanced Algorithms and Architectures for Signal Processing III, San Diego, CA, Aug 1988.

6. C.L. Nikias, and J.M. Mendel (ed). "Workshop on higher-order spectral analysis." Vail, CO, Jun 1989.

7. Naval Civil Engineering Laboratory. Technical Note N-1771: A summary of the SEACON mooring validation experiment, by P.A. Palo and T.P McAllister. Port Hueneme, CA, Jun 1987.

8. J.S. Bendat, and A.G. Piersol. "Spectral analysis of nonlinear systems involving square law operations," Journal of Sound and Vibration, vol 81, 1982.

9. H.J. Rice, and J.A. Fitzpatrick. "A generalized technique for spectral analysis of nonlinear systems," Mechanical Systems and Signal Processing, vol 2, 1988, pp 243-249.

10. H.J. Rice, H. Esmonde, and J.A. Fitzpatrick. "A spectral method for identifying quadratic damping in single degree of freedom systems," in Proceedings, International Symposium on Flow-Induced Vibration and Noise, ASME, vol 3, 1988, pp 269-277.

11. J.J. Stoker. Nonlinear vibrations in mechanical and electrical systems. New York, NY, Interscience Publishers, 1950.

12. F.B. Hildebrand. Advanced calculus for applications. Englewood Cliffs, NJ, Prentice-Hall, 1962.

13. C. Mole, M. Ullman, J. Little, and S. Baugert. 386-Matlab users guide. Sherborn, MA, The Mathworks, Inc., 1987.

14. J.S. Bendat, and A.G. Piersol. Engineering applications of correlation and spectral analysis. New York, NY, Wiley-Interscience, 1980.

15. J.S. Bendat, and A.G. Piersol. Random data: Analysis and measurement procedures, 2nd Ed. New York, NY, Wiley-Interscience, 1986.

SDOF Nonlinear Equations

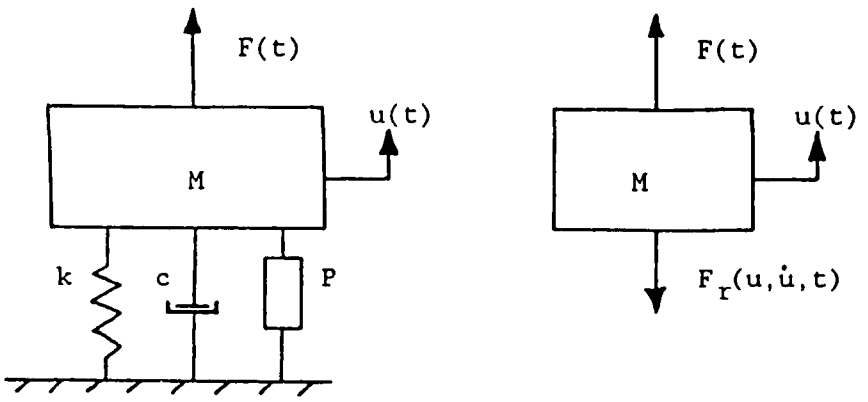

$$M\ddot{u}(t) + C\dot{u}(t) + Ku(t) + P(u,\dot{u},t) = F(t)$$

$$F_r(u,\dot{u},t)$$

where

$$F_r(u,\dot{u},t) = F(t) - M\ddot{u}(t)$$

Figure 1. SDOF nonlinear system and equations.

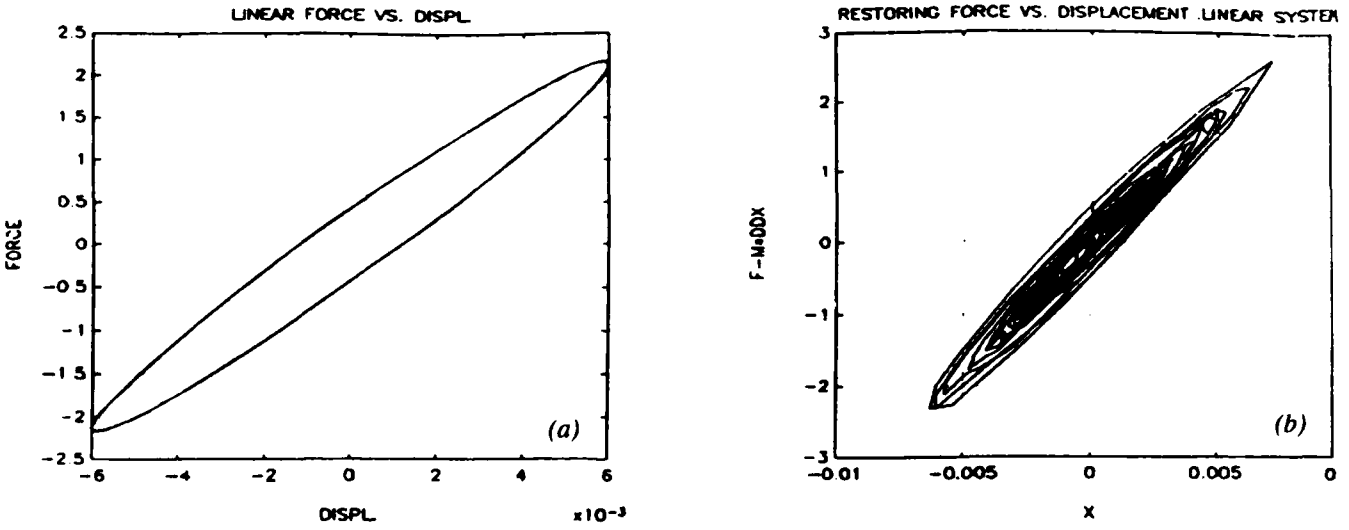

Figure 2. Restoring force/displacement patterns for Linear system.

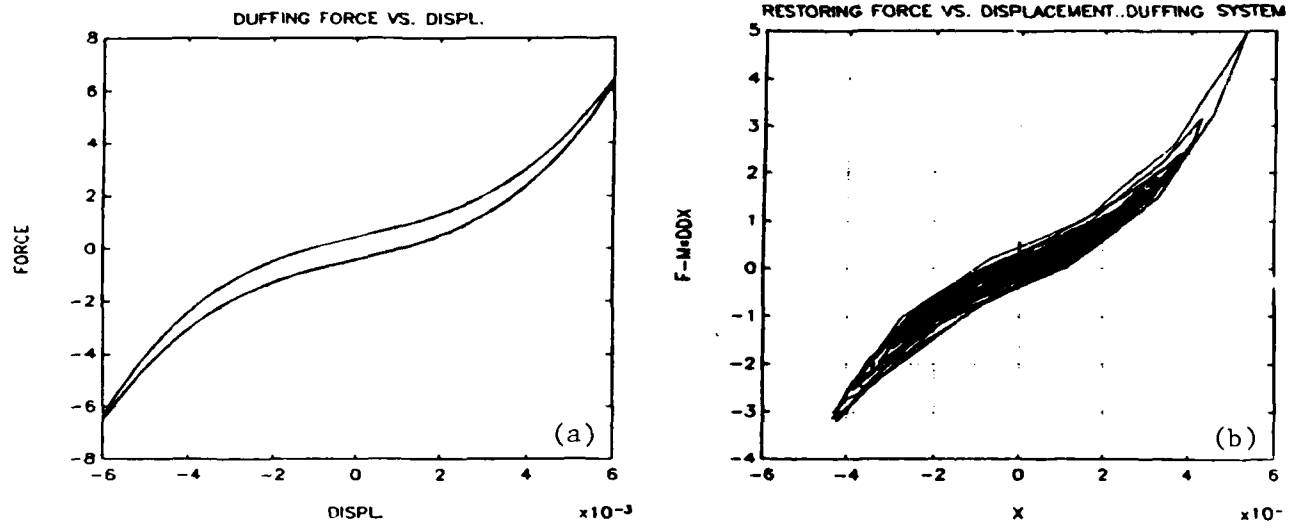

Figure 3. Restoring force/displacement patterns for Duffing system.

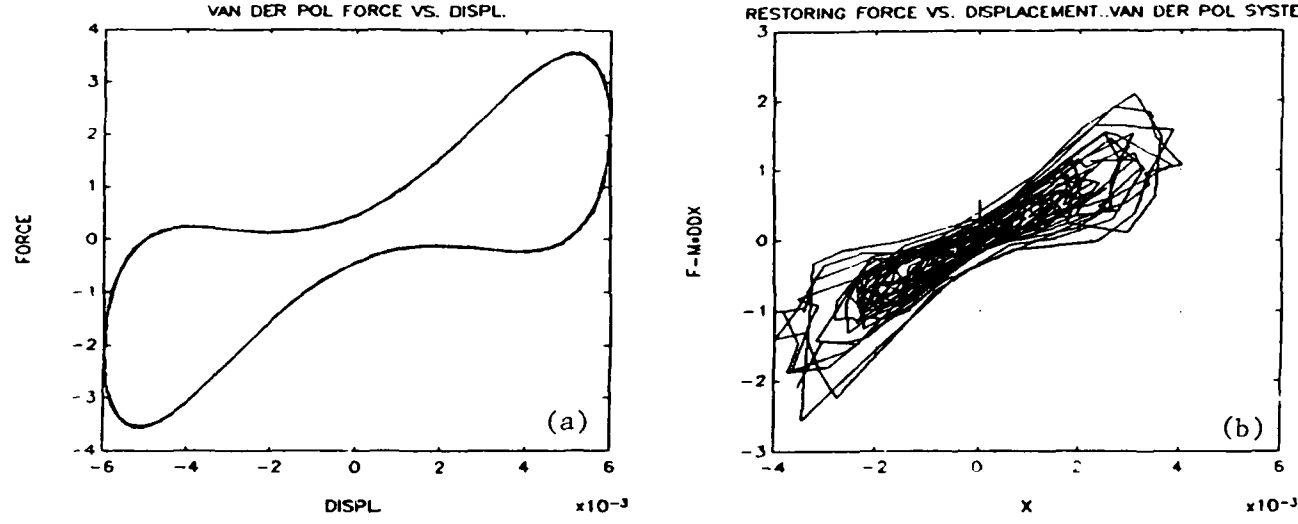

Figure 4. Restoring force/displacement patterns for Van der Pol system.

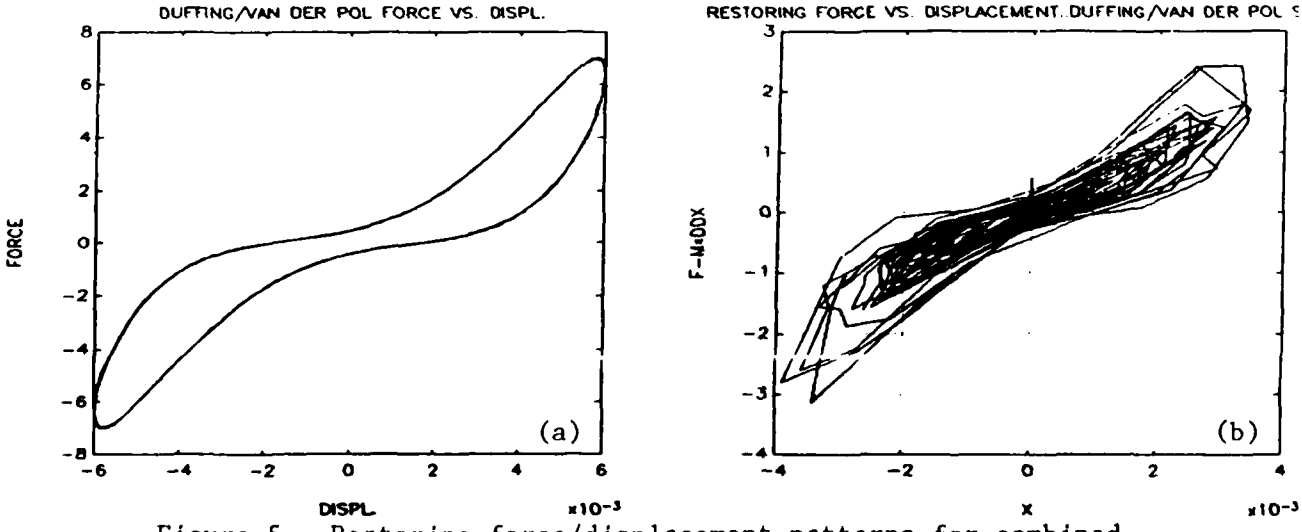

Figure 5. Restoring force/displacement patterns for combined Duffing-Van der Pol system.

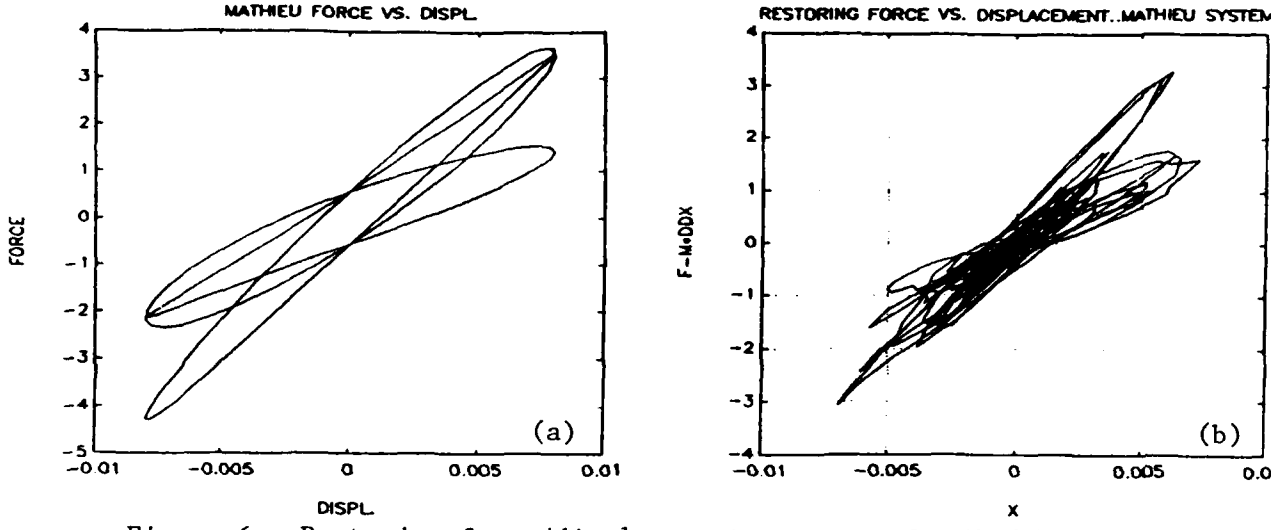

Figure 6. Restoring force/displacement patterns for Mathieu system.

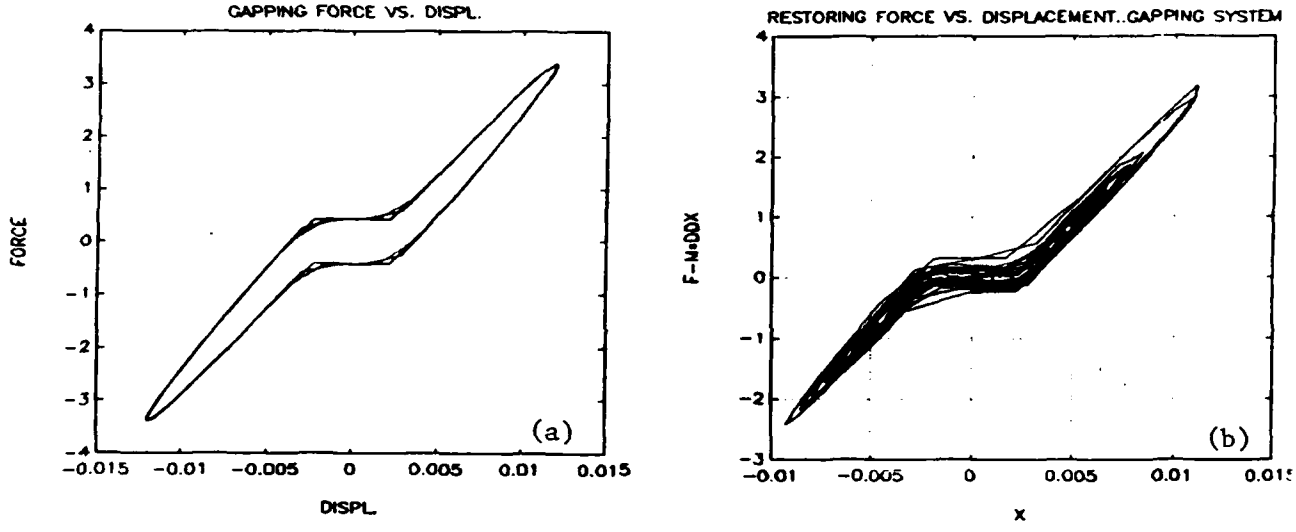

Figure 7. Restoring force/displacement patterns for Dead-Band system.

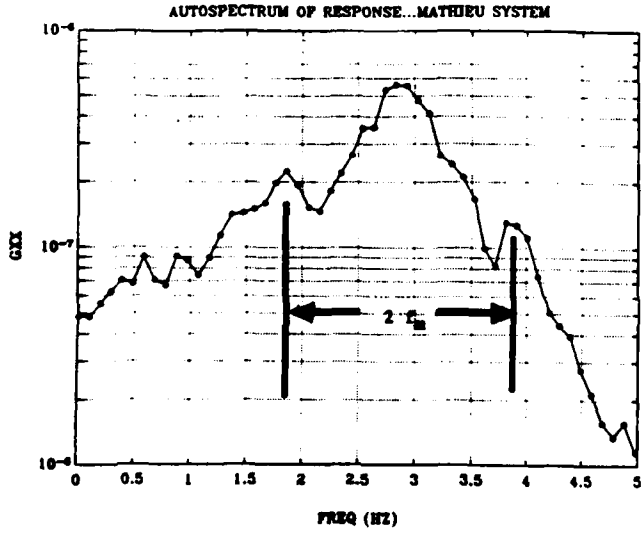

Figure 8. Autospectrum for Mathieu system response.

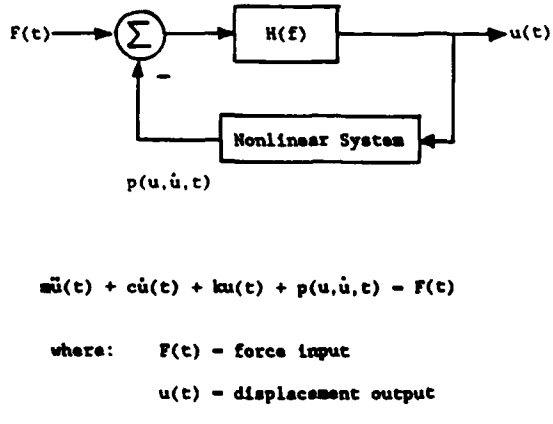

Figure 9. Single-input/single-output nonlinear model with feedback.

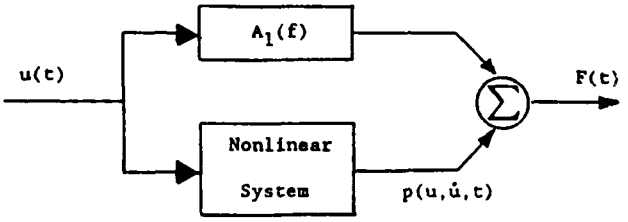

$$m\ddot{u}(t) + c\dot{u}(t) + ku(t) + p(u,\dot{u},t) = F(t)$$

where: u(t) = displacement input

F(t) = force output

Figure 10. Reverse single-input/single-output nonlinear model without feedback.

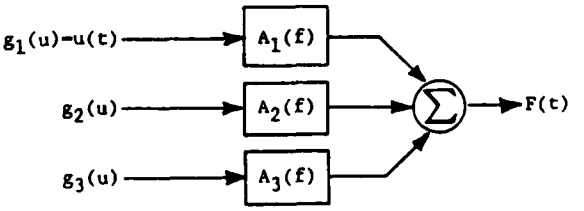

Figure 11. Three-input/single-output linear model where $g_2(u)$ and $g_3(u)$ are zero-memory nonlinear functions of u.

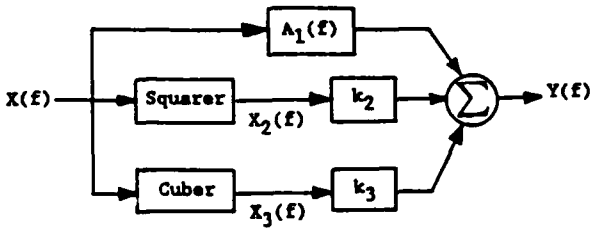

Figure 12. SI/SO nonlinear model where nonlinear stiffness terms have constant coefficients.

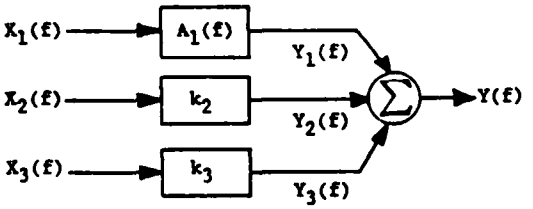

Figure 13. Three-input/single-output linear model where nonlinear stiffness terms have constant coefficients.

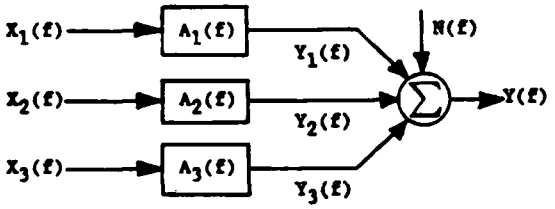

Figure 14. Three-input/single-output linear model where nonlinear stiffness terms have frequency-dependent coefficients.

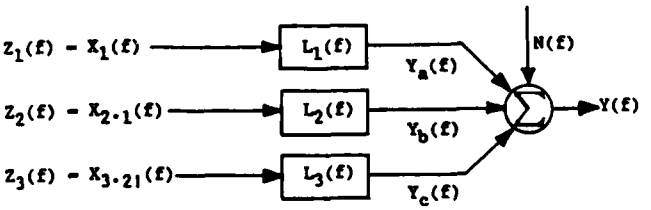

Figure 15. Equivalent three-input/single-output linear model to Figure 14 with uncorrelated inputs.

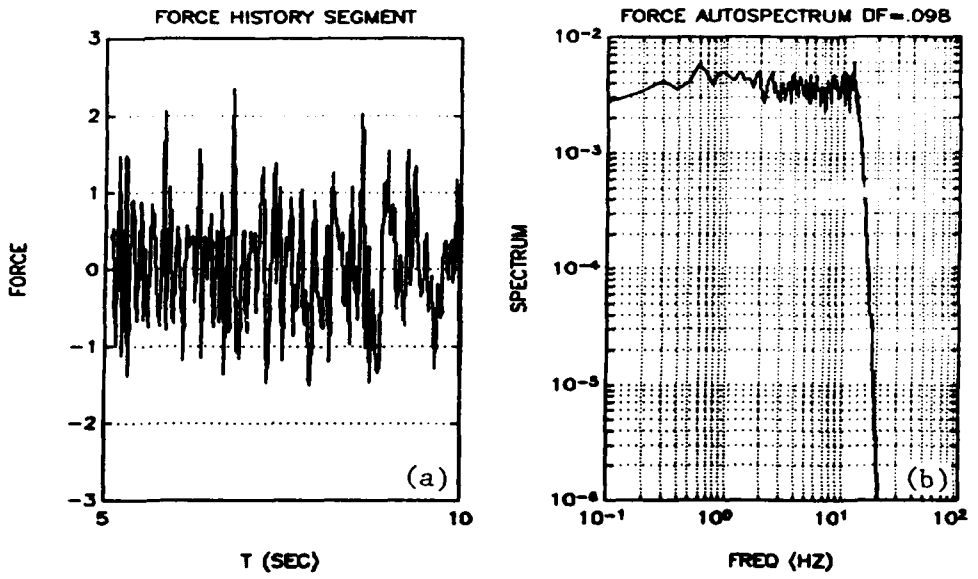

Figure 16. Force history segment and autospectrum.

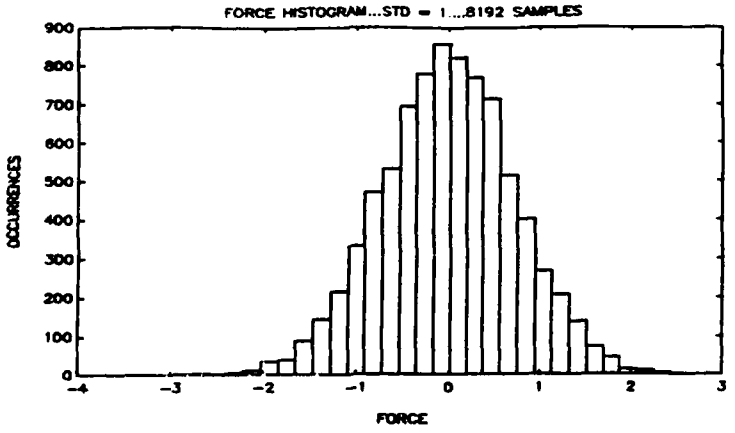

Figure 17. Force histogram.

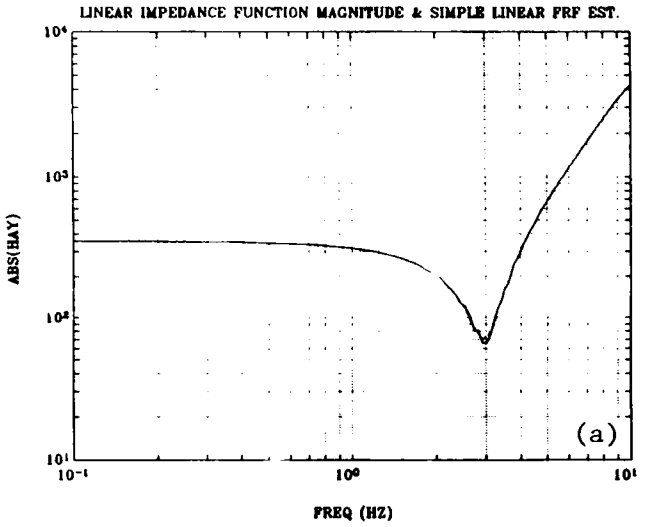

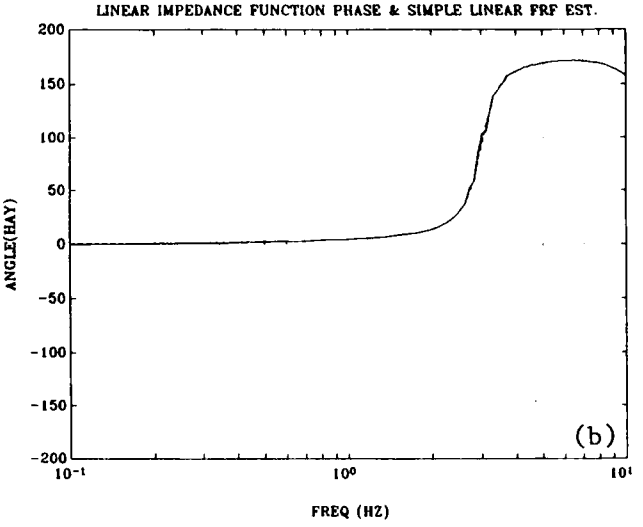

Figure 18. SDOF linear system impedance (magnitude and phase).

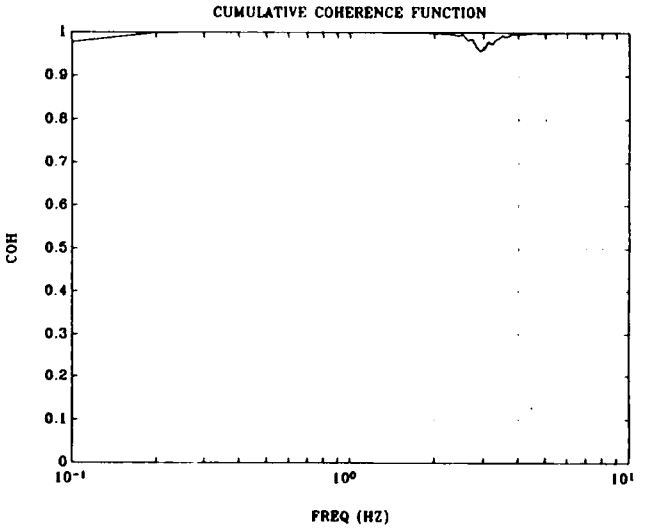

Figure 19. SDOF linear system coherence function.

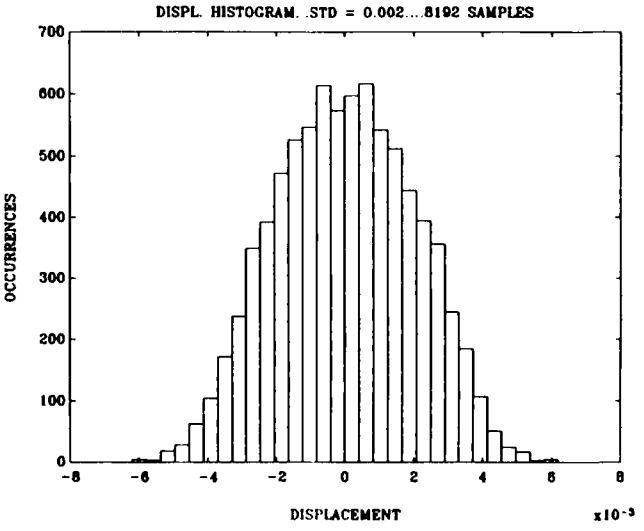

Figure 20. SDOF linear system displacement histogram.

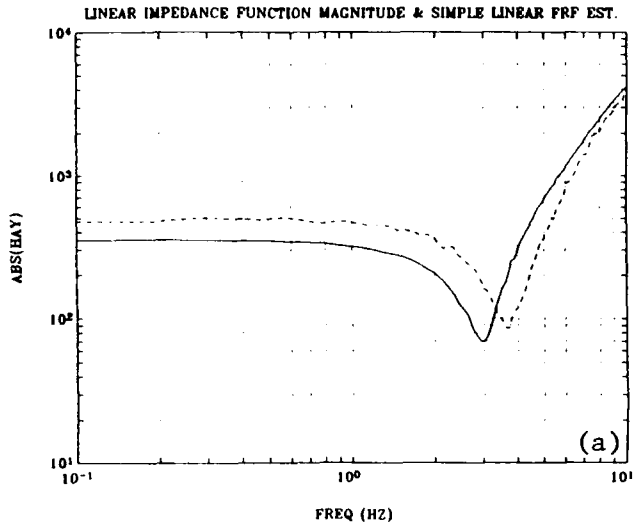

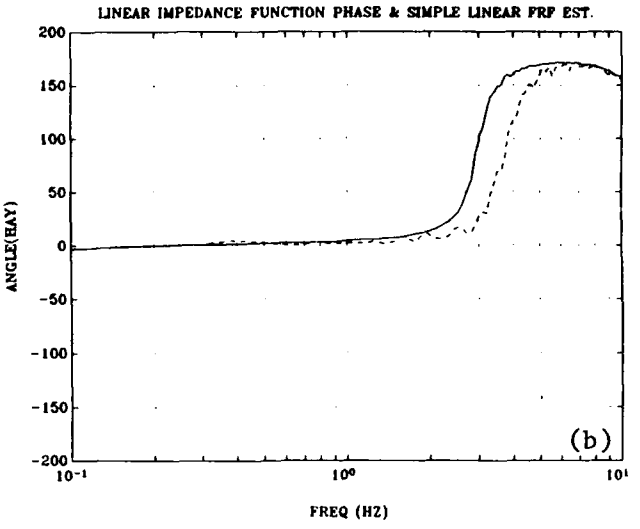

Figure 21. Duffing system linear impedance (magnitude and phase).

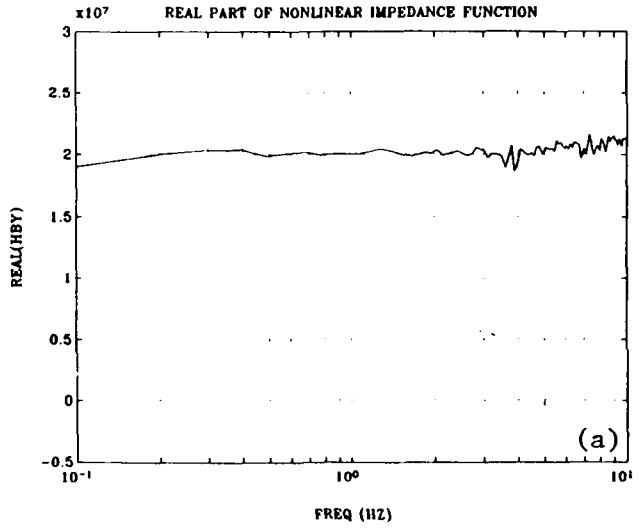

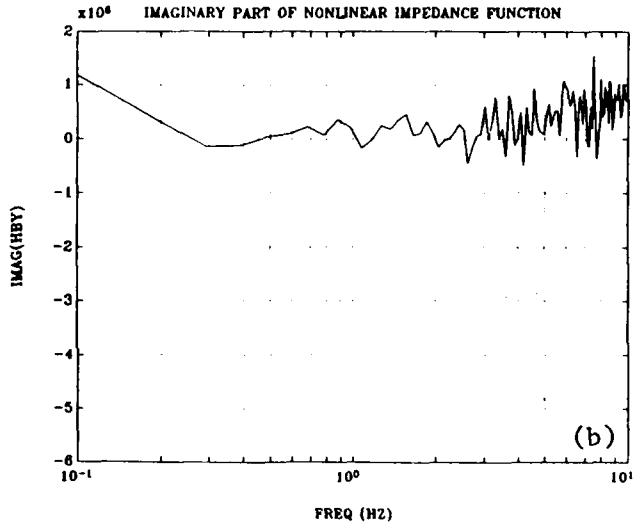

Figure 22. Duffing system nonlinear impedance (real and imaginary).

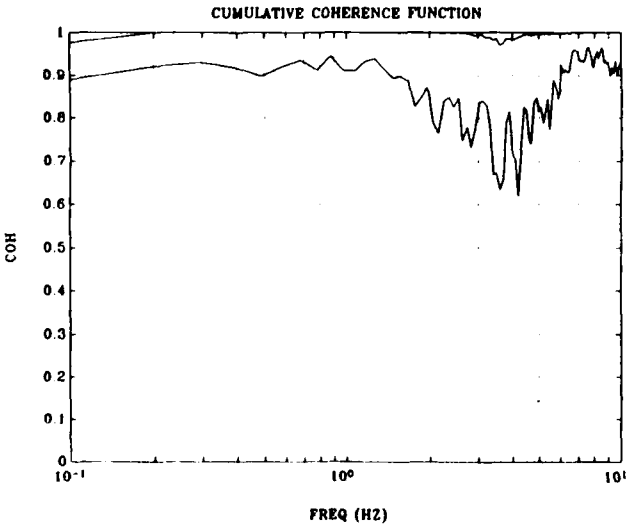

Figure 23. Duffing system cumulative coherence functions.

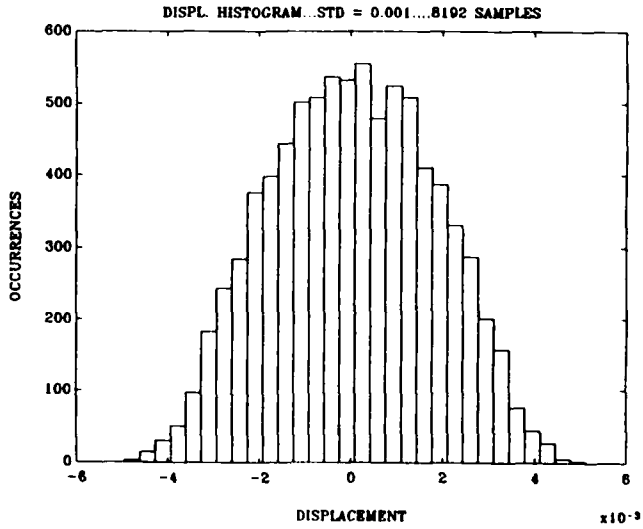

Figure 24. Duffing system displacement histogram.

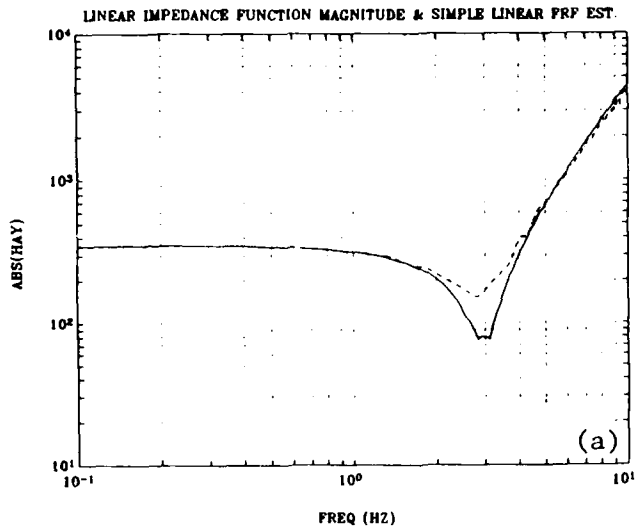

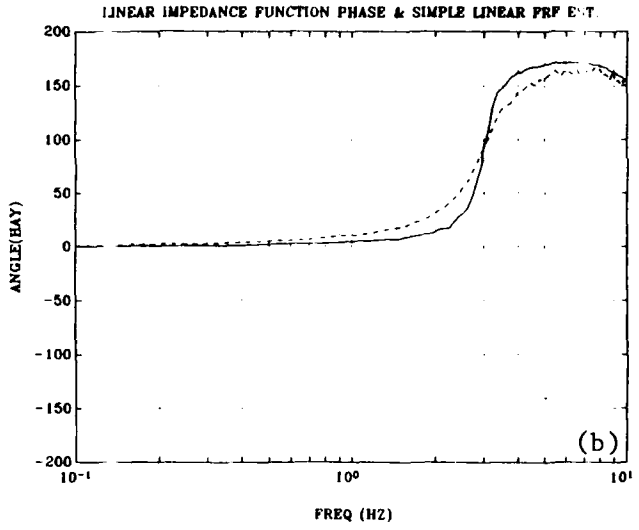

Figure 25. Van der Pol system linear impedance (magnitude and phase).

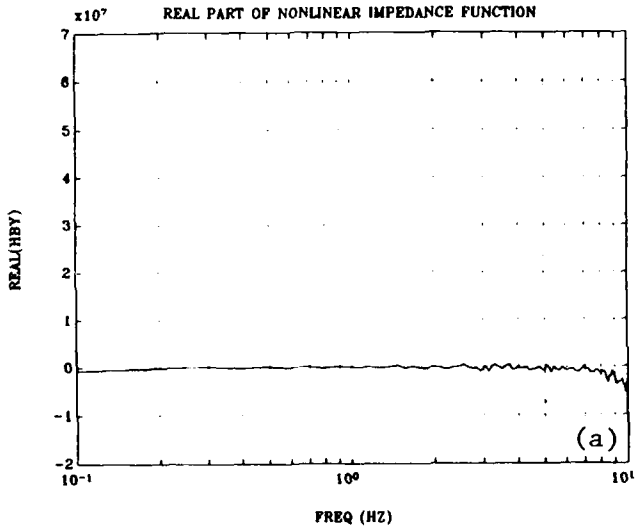

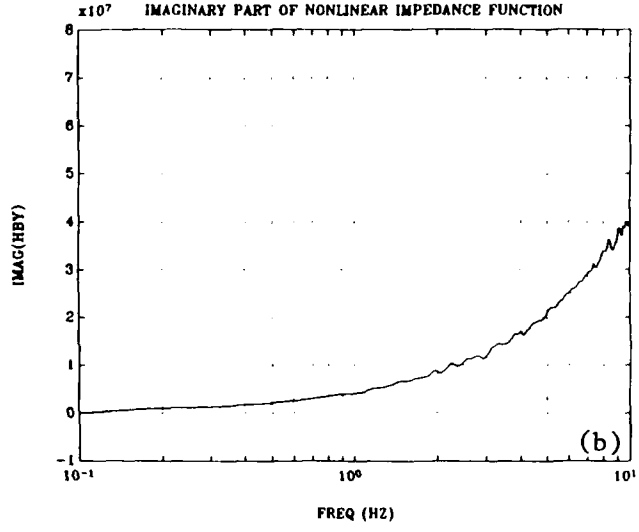

Figure 26. Van der Pol system nonlinear impedance (real and imaginary).

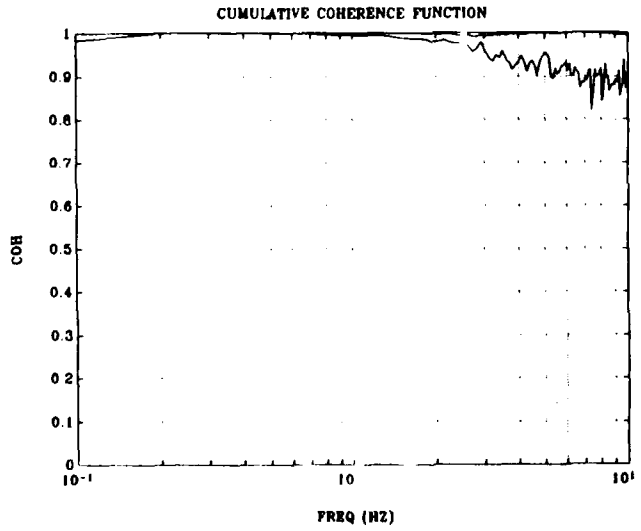

Figure 27. Van der Pol system cumulative coherence functions.

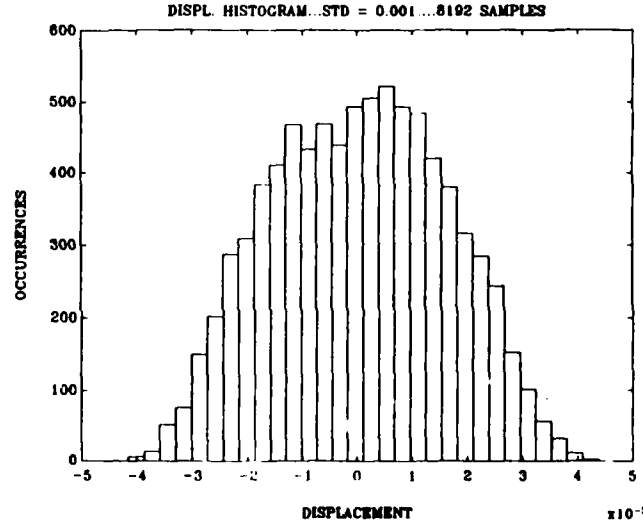

Figure 28. Van der Pol system displacement histogram.

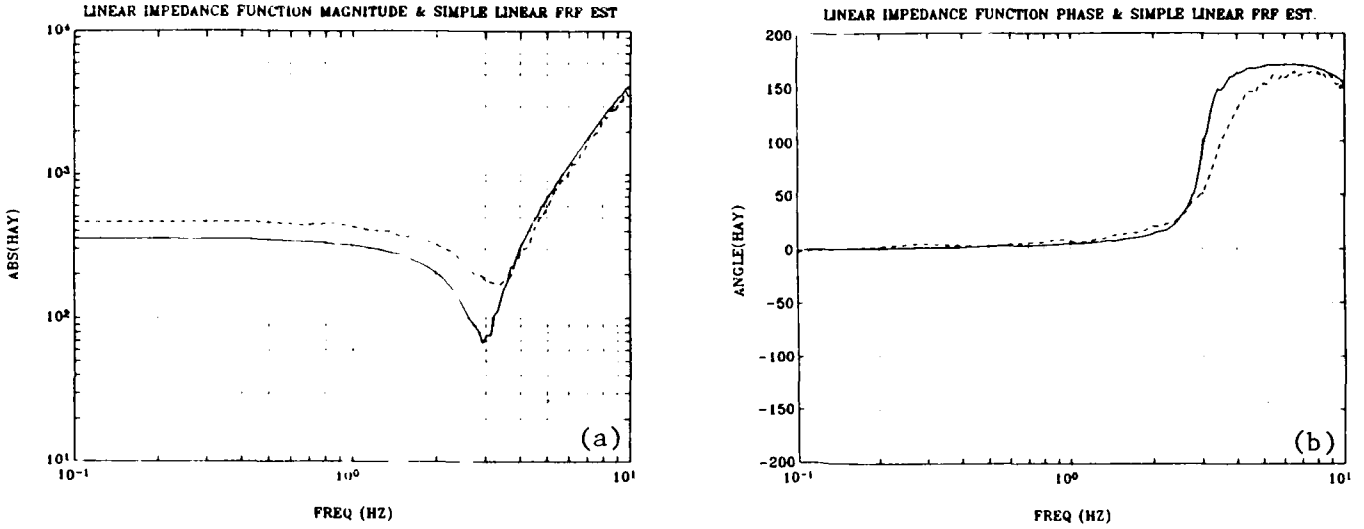

Figure 29. Combined Duffing-Van der Pol system linear impedance (magnitude and phase).

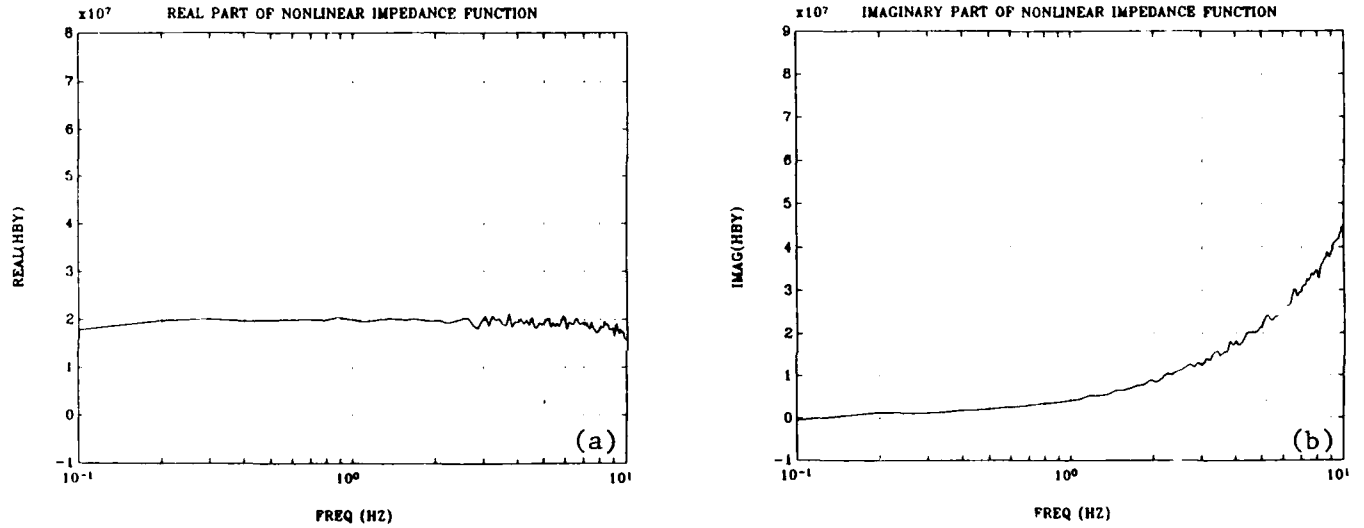

Figure 30. Combined Duffing-Van der Pol system nonlinear impedance (real and imaginary).

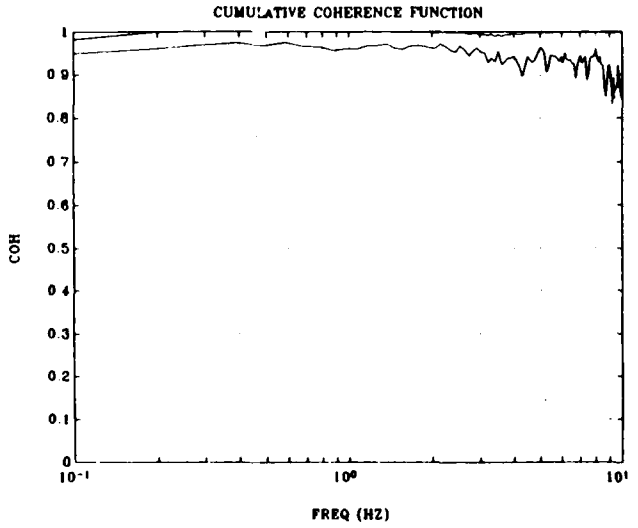

Figure 31. Combined Duffing-Van der Pol system cumulative coherence functions.

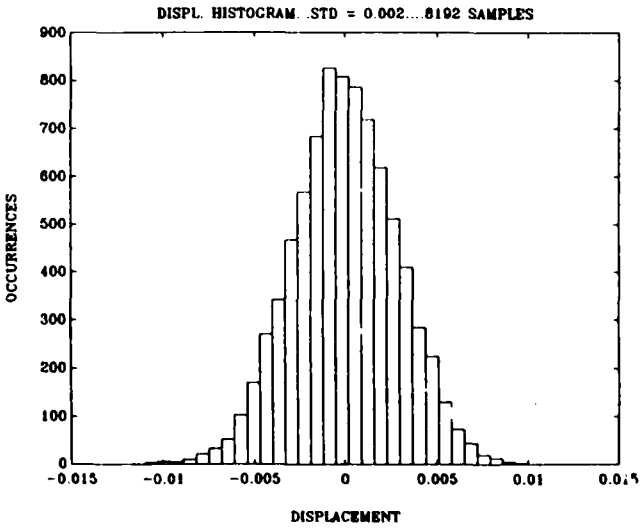

Figure 32. Combined Duffing-Van der Pol system displacement histogram.

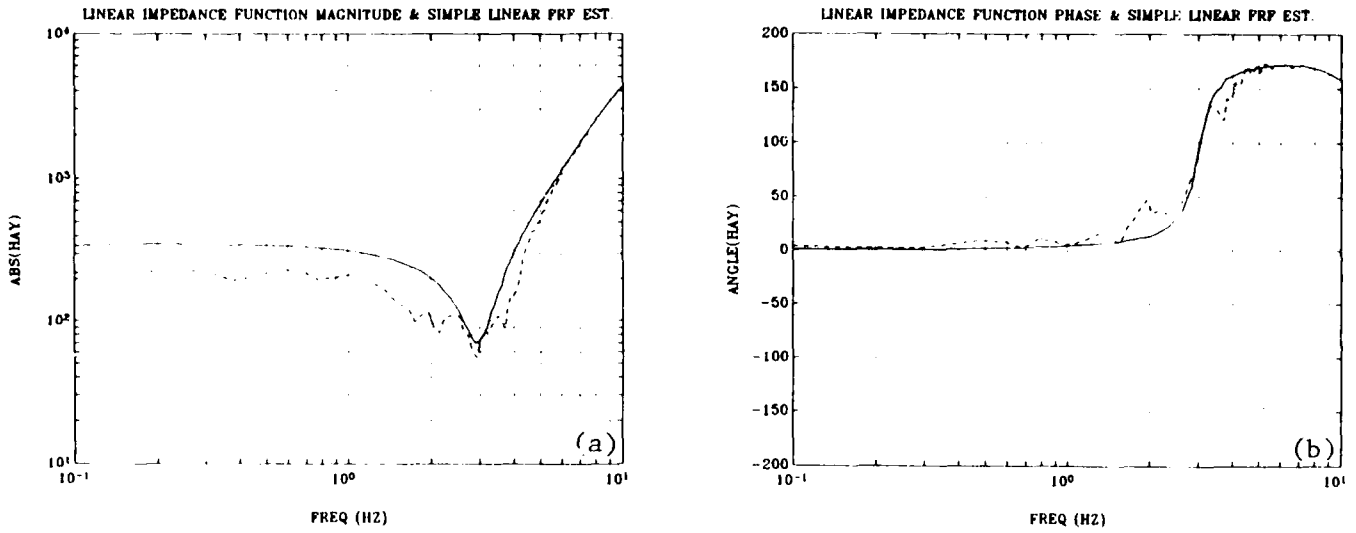

Figure 33. Mathieu system linear impedance (magnitude and phase).

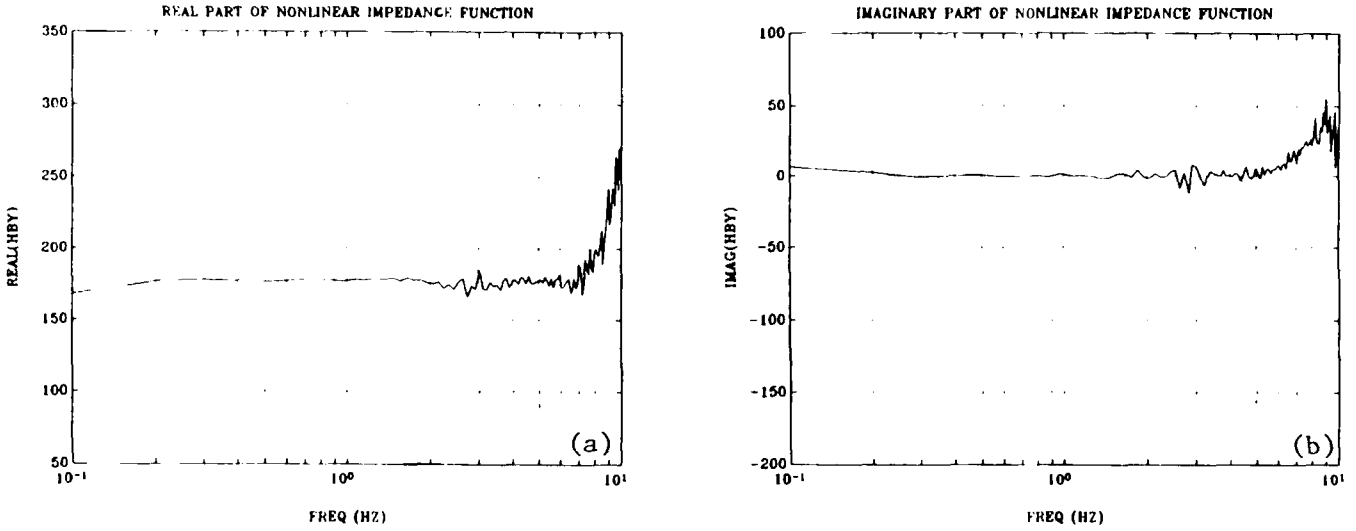

Figure 34. Mathieu system nonlinear impedance (real and imaginary).

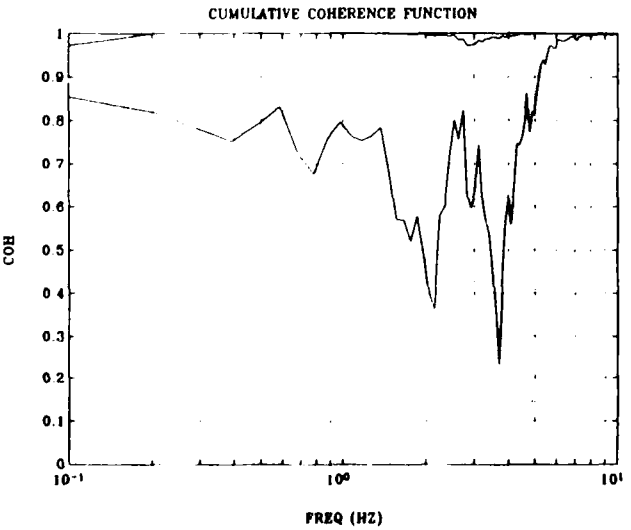

Figure 35. Mathieu system cumulative coherence functions.

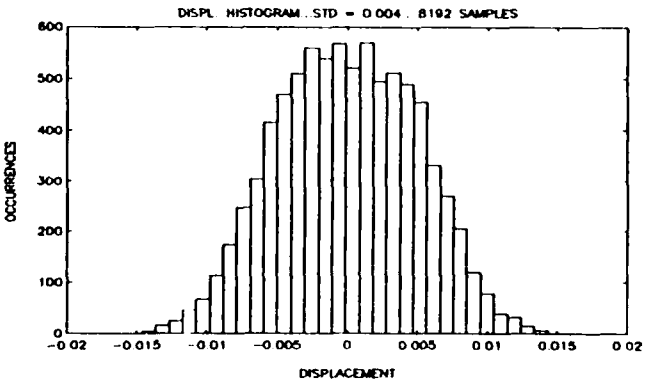

Figure 36. Mathieu system displacement histogram.

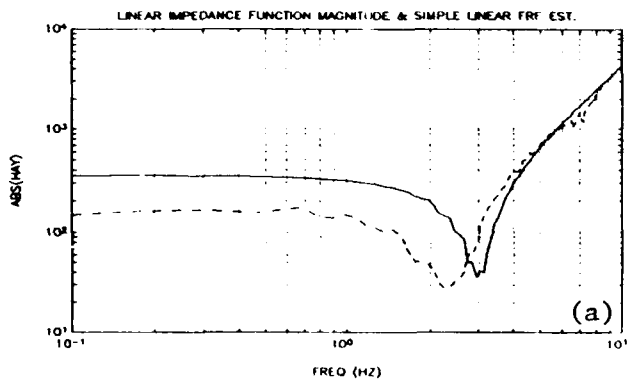

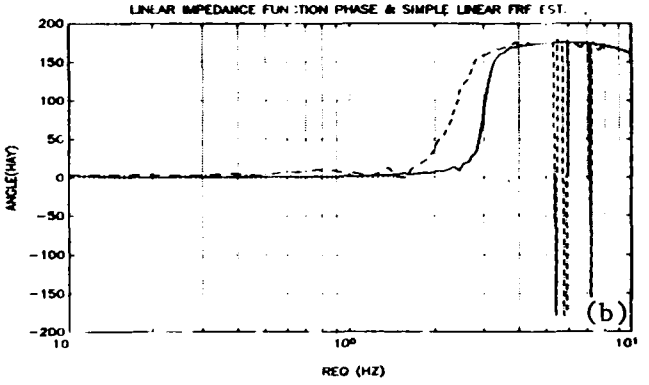

Figure 37. Dead-Band system linear impedance (magnitude and phase).

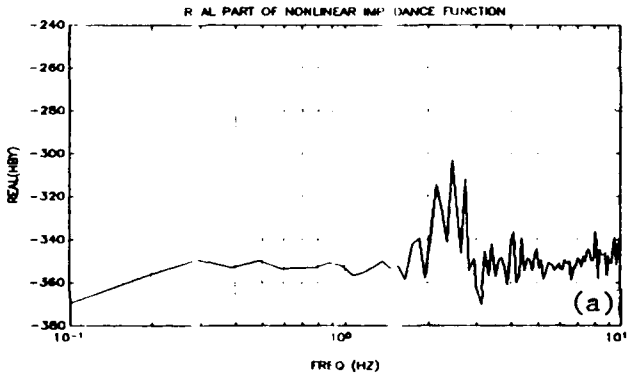

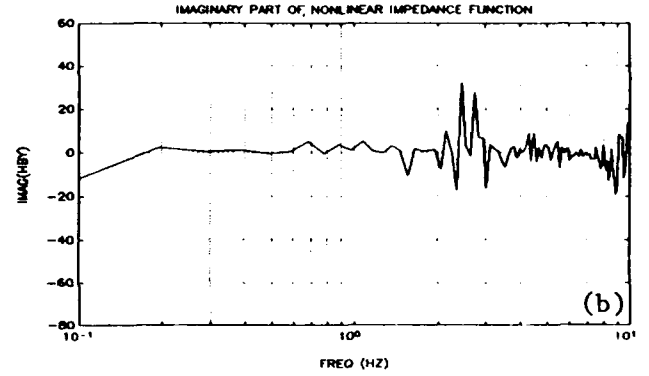

Figure 38. Dead-Band system nonlinear impedance (real and imaginary).

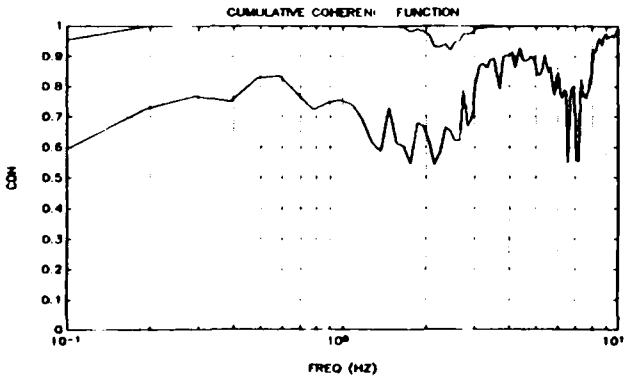

Figure 39. Dead-Band system cumulative coherence functions.

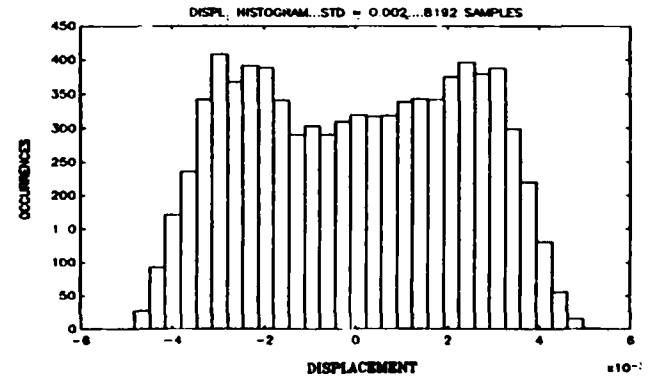

Figure 40. Dead-Band system displacement histogram.

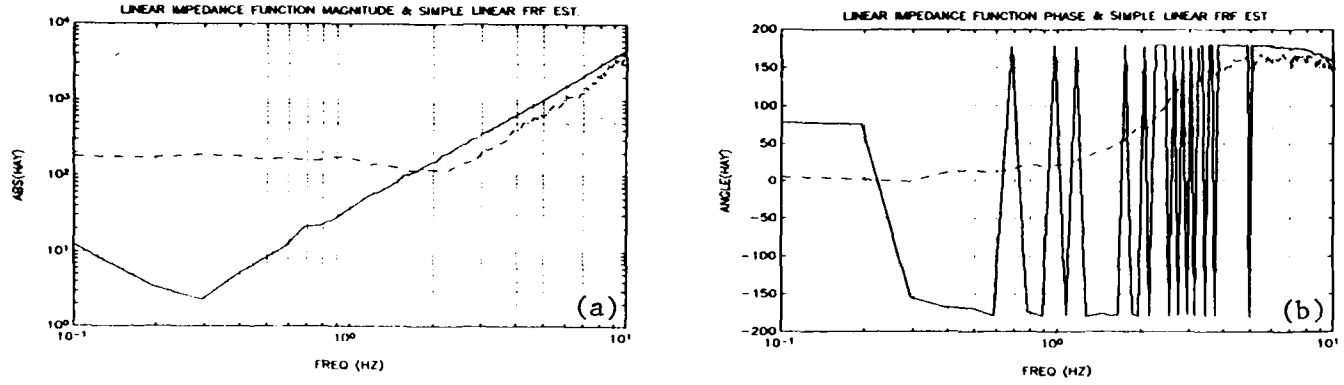

Figure 41. Extreme D-VdP system linear impedance (magnitude and phase).

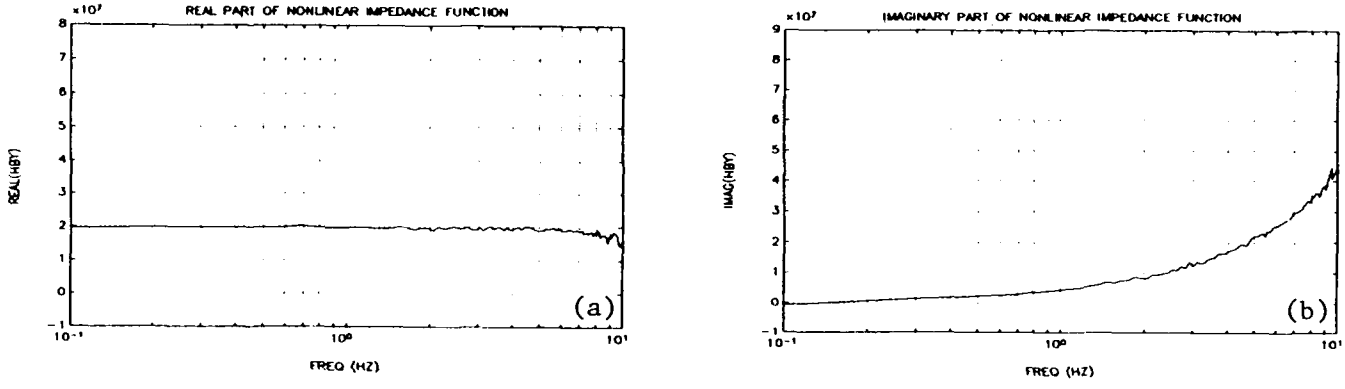

Figure 42. Extreme D-VdP system nonlinear impedance (real and imaginary).

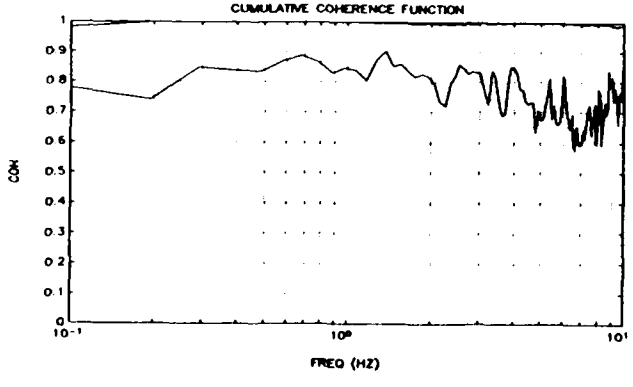

Figure 43. Extreme D-VdP system cumulative coherence functions.

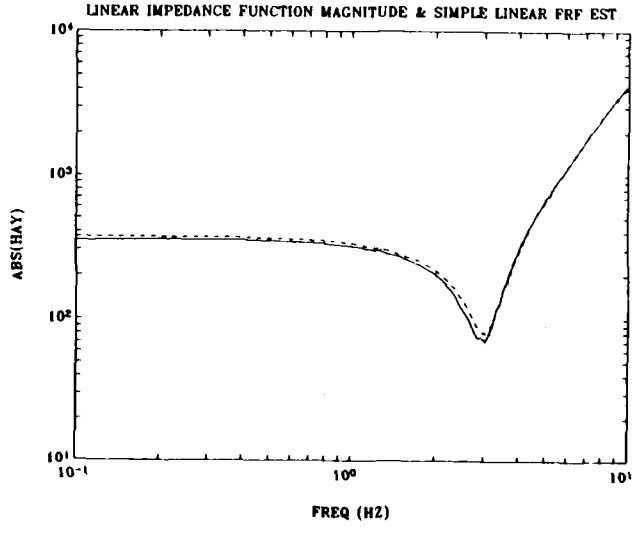

Figure 44. Linear impedance magnitude for 0.2 input variance.

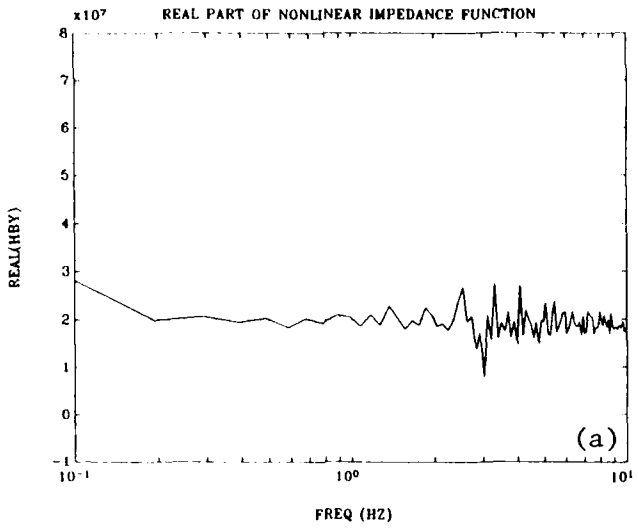

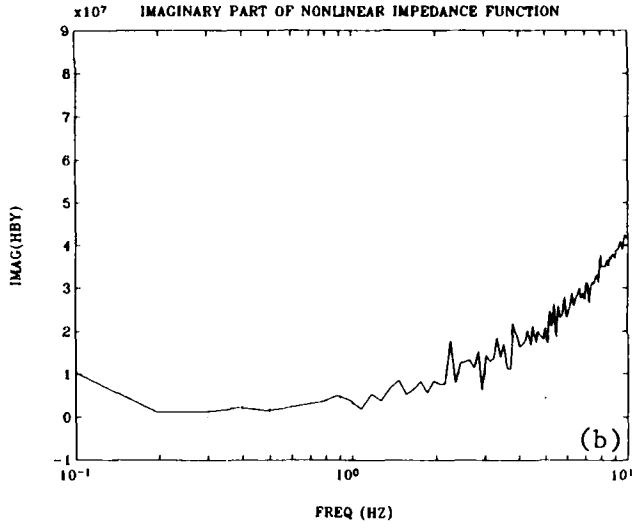

Figure 45. Nonlinear impedance real and imaginary for 0.2 input variance.

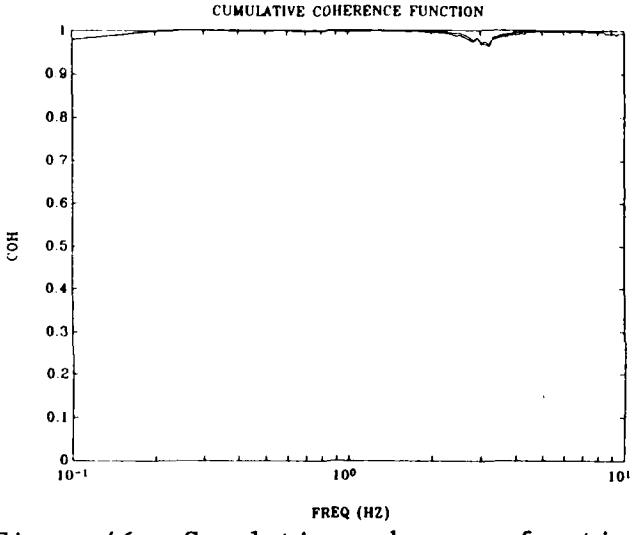

Figure 46. Cumulative coherence functions for 0.2 input variance.

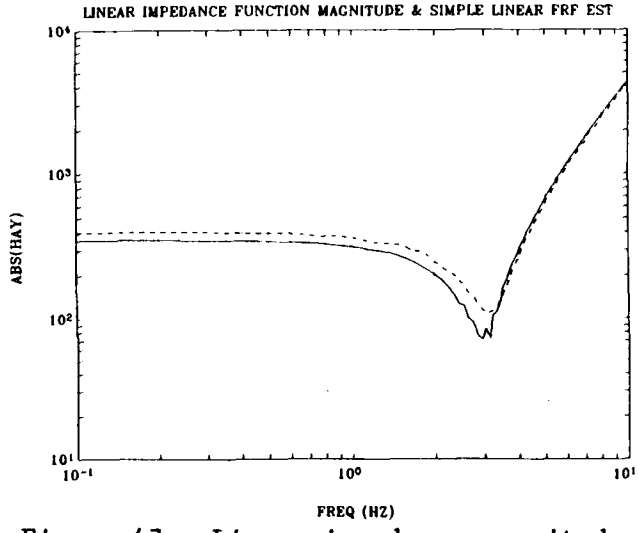

Figure 47. Linear impedance magnitude for 0.5 input variance.

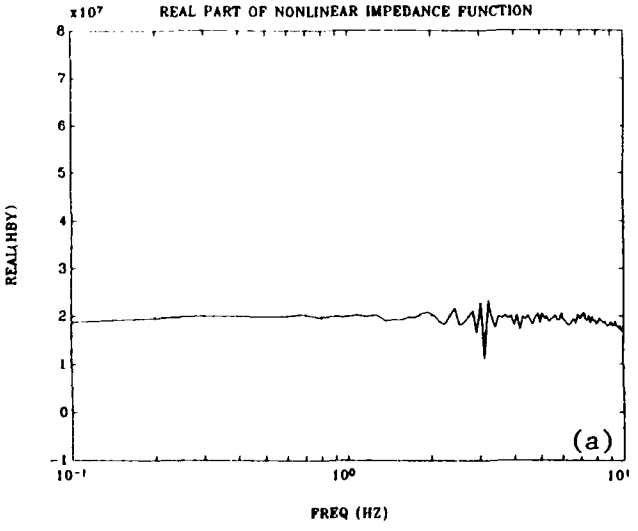

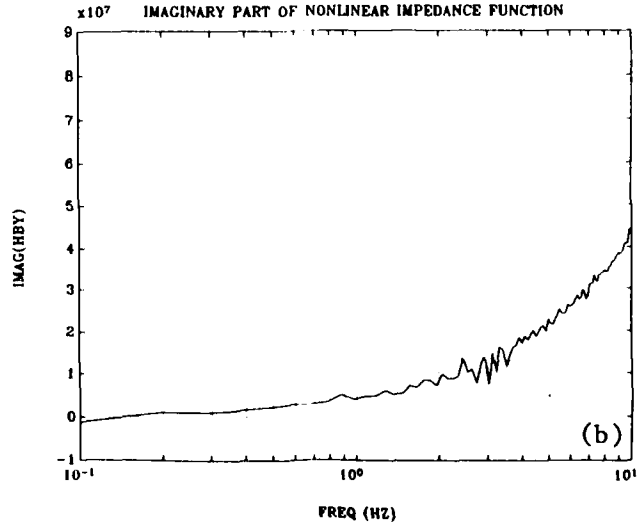

Figure 48. Nonlinear impedance real and imaginary for 0.5 input variance.

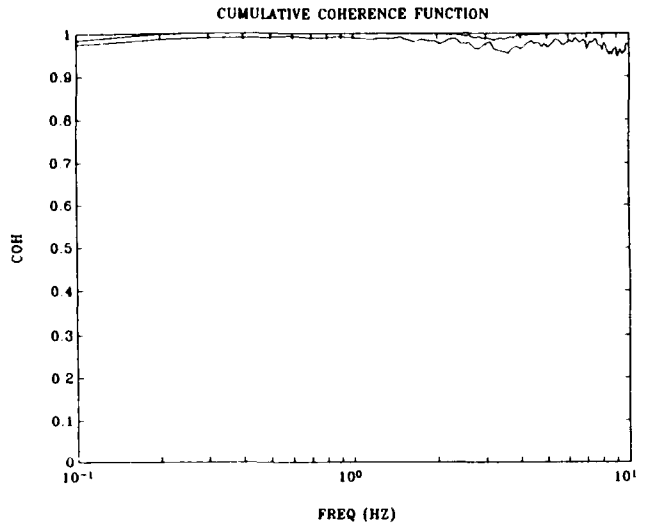

Figure 49. Cumulative coherence functions for 0.5 input variance.

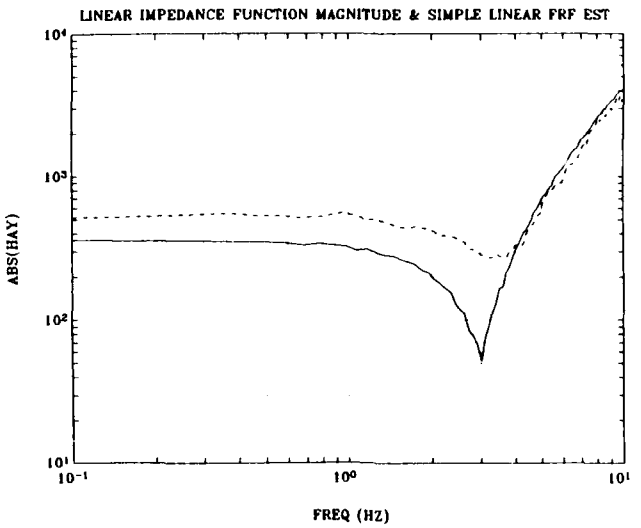

Figure 50. Linear impedance magnitude for 2.0 input variance.

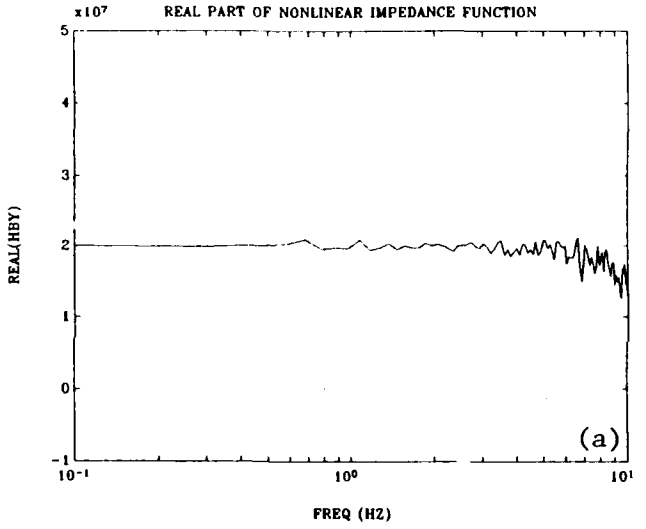

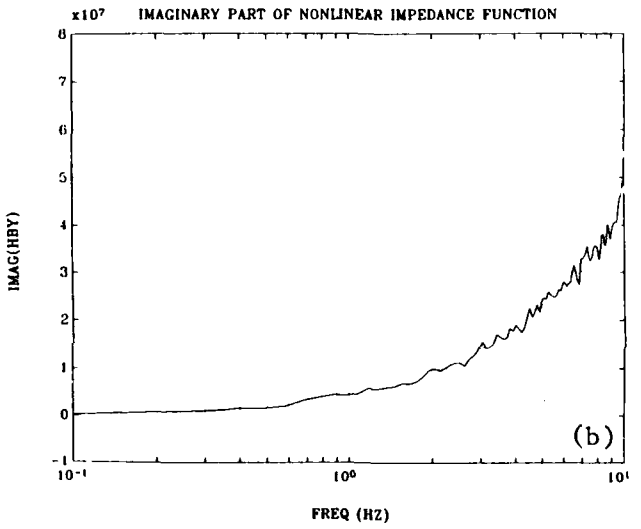

Figure 51. Nonlinear impedance real and imaginary for 2.0 input variance.

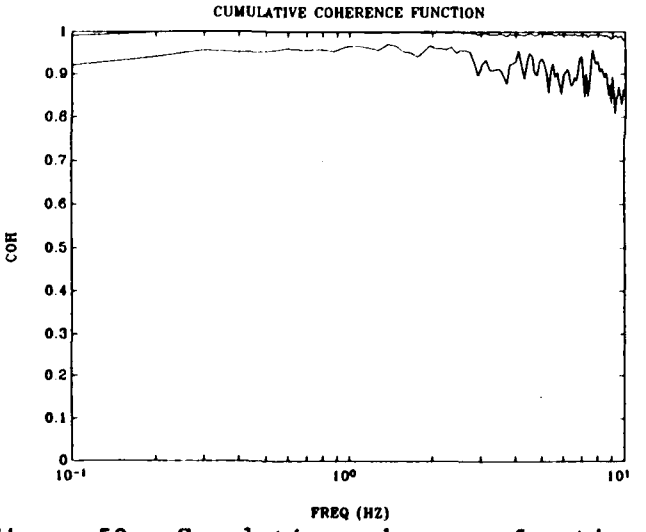

Figure 52. Cumulative coherence functions for 2.0 input variance.

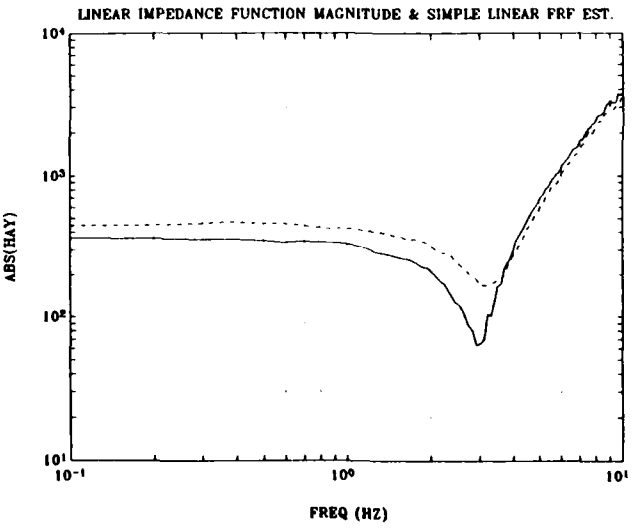

Figure 53. Linear impedance magnitude for 5% noise.

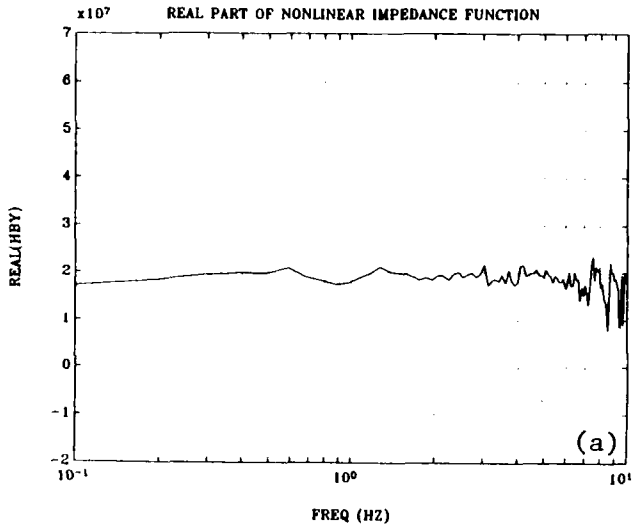

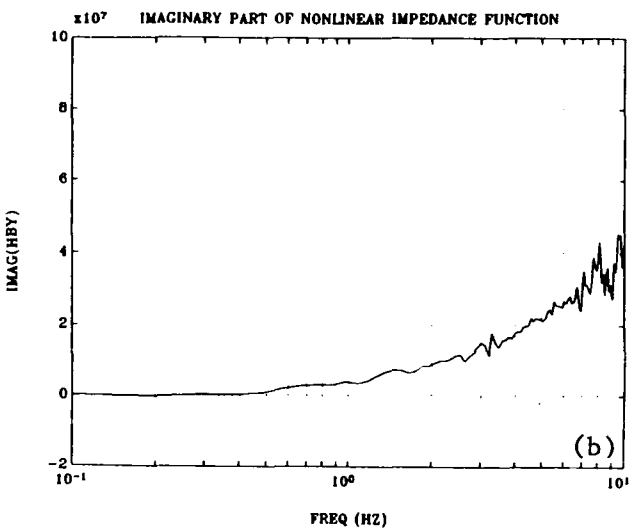

Figure 54. Nonlinear impedance real and imaginary for 5% noise.

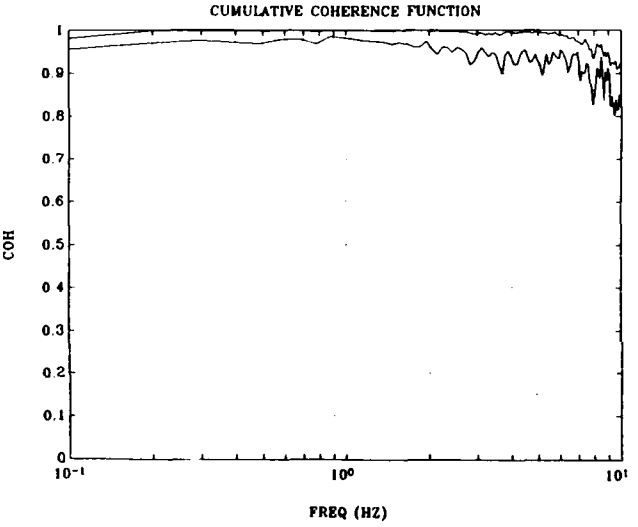

Figure 55. Cumulative coherence functions for 5% noise.

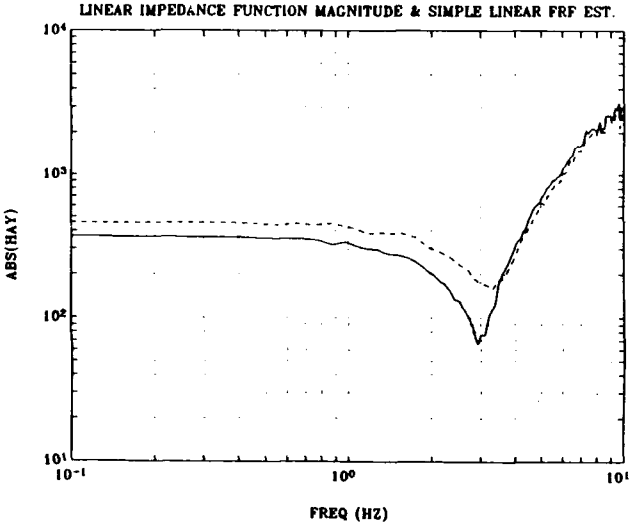

Figure 56. Linear impedance magnitude for 10% noise.

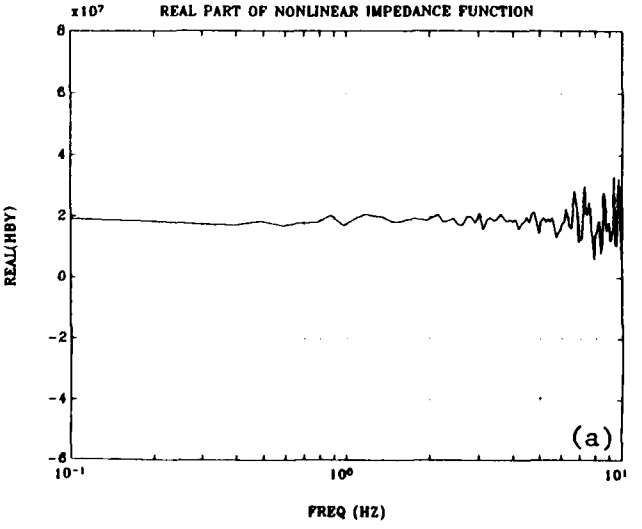

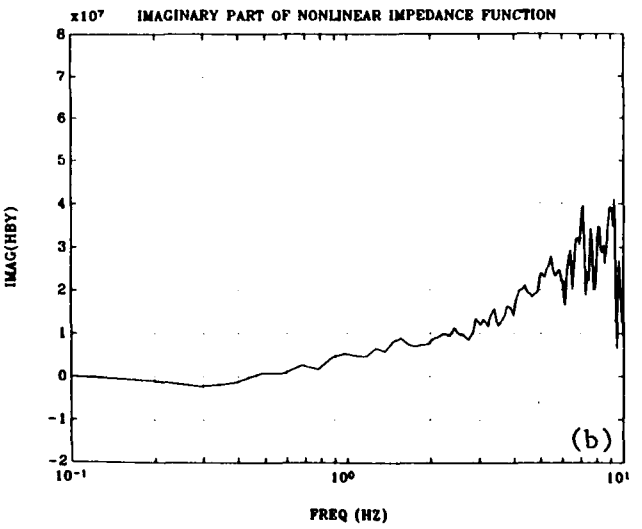

Figure 57. Nonlinear impedance real and imaginary for 10% noise.

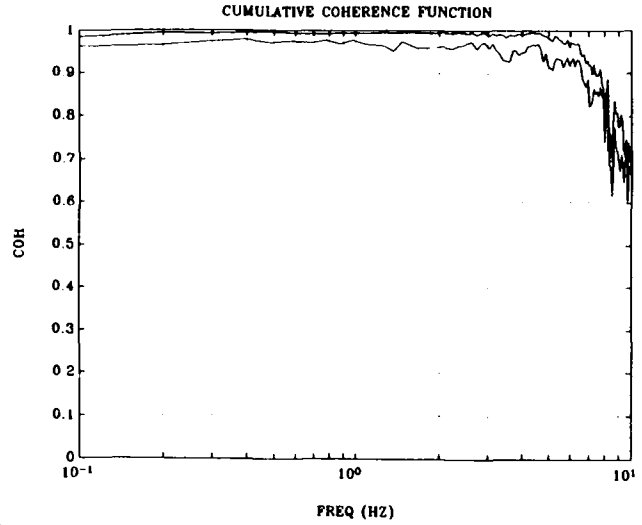

Figure 58. Cumulative coherence functions for 10% noise.

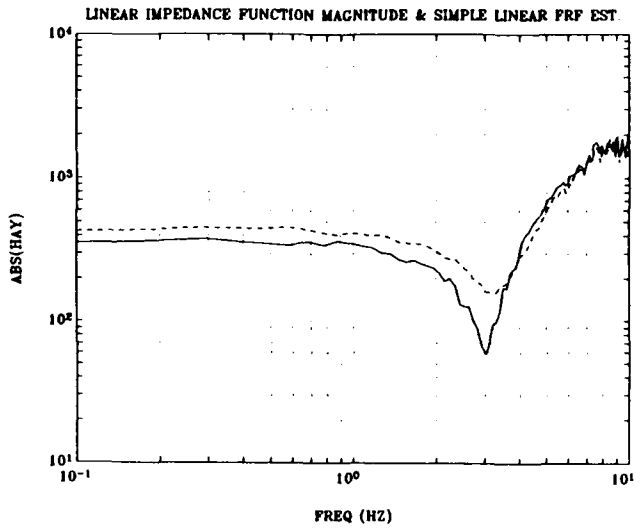

Figure 59. Linear impedance magnitude for 20% noise.

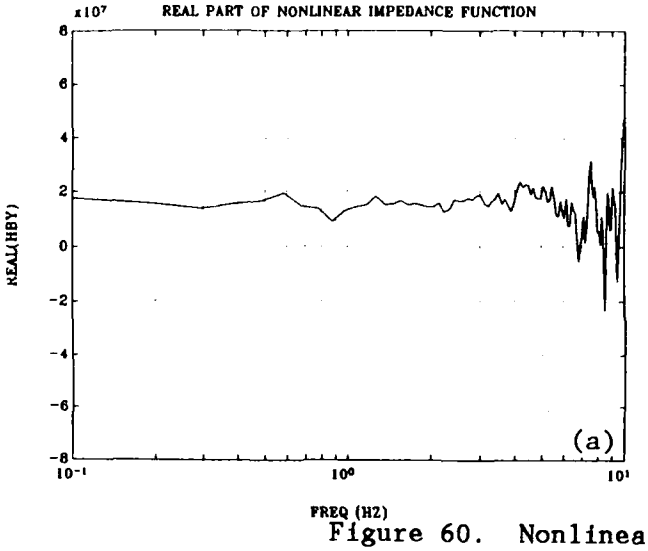

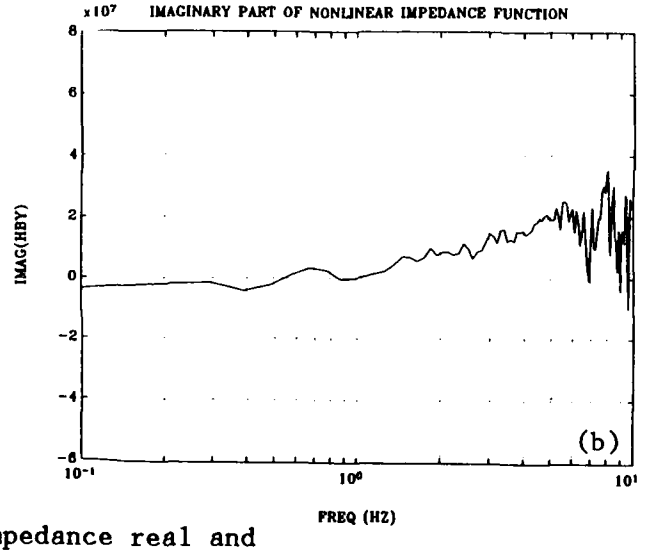

Figure 60. Nonlinear impedance real and imaginary for 20% noise.

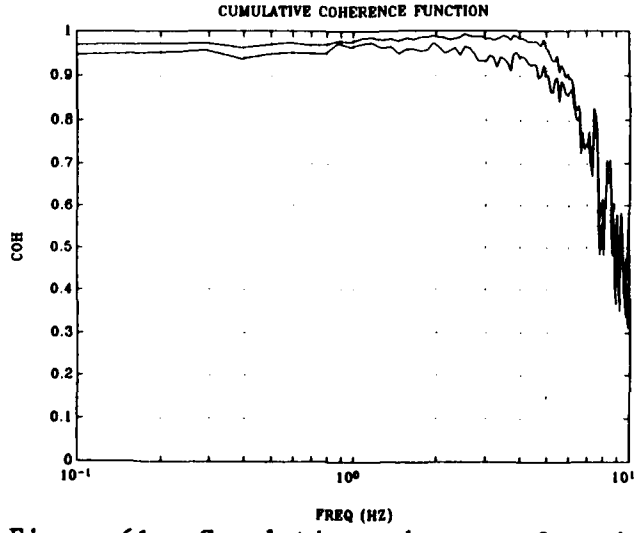

Figure 61. Cumulative coherence functions for 20% noise.

DISTRIBUTION LIST

ARMY R&D Lab, STRNC-UE, Natick, MA
ARMY EWES Library, Vicksburg MS
COGARD R&DC Library, Groton, CT
DIRSSP Tech Lib, Washington, DC
DOE Wind/Ocean Tech Div, Tobacco, MD
DTIC Alexandria, VA
GIDEP OIC, Corona, CA
LIBRARY OF CONGRESS Sci & Tech Div, Washington, DC
NAVCOASTSYSCEN Tech Library, Panama City, FL
NAVOCEANSYSCEN Code 9642B, San Diego, CA; DET, Tech Lib, Kailua, HI
NAVPGSCOL Code 1424, Library, Monterey, CA
NAVSEASYSCOM Code 56W23 (J Coon), Washington, DC
NAVSTA SCE, San Diego, CA
NOAA Data Buoy Off, Engrg Div, Bay St. Louis, MS; Library, Rockville, MD
NRL Code 2511, Washington, DC
NUSC DET Lib (Code 4533), Newport, RI
PMTC Code 1018, Point Mugu, CA
USNA Ocean Engrg Dept (McCormick), Annapolis, MD
CALIFORNIA INSTITUTE OF TECHNOLOGY Environ Engrg Lib, Pasadena, CA
CORNELL UNIVERSITY Library, Ithaca, NY
DAMES & MOORE Library, Los Angeles, CA
DUKE UNIVERSITY CE Dept (Muga), Durham, NC
INSTITUTE OF MARINE SCIENCES Library, Port Aransas, TX
LEHIGH UNIVERSITY Linderman Library, Bethlehem, PA
MIT Engrg Lib, Cambridge, MA; Lib, Tech Reports, Cambridge, MA; Ocean Engrg Dept (Vandiver), Cambridge, MA
OREGON STATE UNIVERSITY CE Dept (Yim), Corvallis, OR
PENNSYLVANIA STATE UNIVERSITY Applied Rsch Lab, State College, PA
PURDUE UNIVERSITY Engrg Lib, W. Lafayette, IN
STATE UNIVERSITY OF NEW YORK CE Dept, Buffalo, NY
TEXAS A&M UNIVERSITY Ocean Engr Proj, College Station, TX
UNIVERSITY OF ALASKA Biomed & Marine Sci Lib, Fairbanks, AK
UNIVERSITY OF CALIFORNIA Naval Archt Dept, Berkeley, CA
UNIVERSITY OF DELAWARE CE Dept, Ocean Engrg (Dalrymple), Newark, DE
UNIVERSITY OF HAWAII Manoa, Library, Honolulu, HI
UNIVERSITY OF ILLINOIS Library, Urbana, IL
UNIVERSITY OF RHODE ISLAND Pell Marine Sci Lib, Narragansett, RI
UNIVERSITY OF SO CALIFORNIA Hancock Library, Los Angeles, CA
UNIVERSITY OF WASHINGTON Applied Phy Lab Lib, Seattle, WA
BATTELLE New Eng Marine Rsch Lab, Lib, Duxbury, MA
CANADA Viateur De Champlain, D.S.A., Matane, Quebec
GOULD INC. Ches Instru Div. Tech Lib, Glen Burnie, MD
HUGHES AIRCRAFT CO Tech Doc Cen, El Segundo, CA
MC CLELLAND ENGRS, INC Library, Houston, TX
MOBIL R&D CORP Offshore Engrg Lib, Dallas, TX
NATL ACADEMY OF ENGRG Alexandria, VA
SANDIA LABS Library, Livermore, CA
WESTINGHOUSE ELECTRIC CORP Oceanic Div Lib, Annapolis, MD
WOODWARD-CLYDE CONSULTANTS West Reg, Lib, Oakland, CA
HERONEMUS, W.E. Amherst, MA

INSTRUCTIONS

The Naval Civil Engineering Laboratory has revised its primary distribution lists. The bottom of the label on the reverse side has several numbers listed. These numbers correspond to numbers assigned to the list of Subject Categories. Numbers on the label corresponding to those on the list indicate the subject category and type of documents you are presently receiving. If you are satisfied, throw this card away (or file it for later reference).

If you want to change what you are presently receiving:

- Delete - mark off number on bottom of label.
- Add - circle number on list.
- Remove my name from all your lists - check box on list.
- Change my address - line out incorrect line and write in correction **(DO NOT REMOVE LABEL).**
- Number of copies should be entered after the title of the subject categories you select.

Fold on line below and drop in the mail.

Note: Numbers on label but not listed on questionnaire are for NCEL use only. please ignore them.

Fold on line and staple.

DEPARTMENT OF THE NAVY

Naval Civil Engineering Laboratory
Port Hueneme, CA 93043-5003

Official Business
Penalty for Private Use, $300

NO POSTAGE
NECESSARY
IF MAILED
IN THE
UNITED STATES

BUSINESS REPLY CARD

FIRST CLASS PERMIT NO. 12503 WASH D.C.

POSTAGE WILL BE PAID BY ADDRESSEE

Commanding Officer
Code L34
Naval Civil Engineering Laboratory
Port Hueneme, California 93043-5003

DISTRIBUTION QUESTIONNAIRE

The Naval Civil Engineering Laboratory is revising its Primary distribution lists.

SUBJECT CATEGORIES

1 SHORE FACILITIES
2 Construction methods and materials (including corrosion control, coatings)
3 Waterfront structures (maintenance/deterioration control)
4 Utilities (including power conditioning)
5 Explosives safety
6 Aviation Engineering Test Facilities
7 Fire prevention and control
8 Antenna technology
9 Structural analysis and design (including numerical and computer techniques)
10 Protective construction (including hardened shelters, shock and vibration studies)
11 Soil/rock mechanics
14 Airfields and pavements

15 ADVANCED BASE AND AMPHIBIOUS FACILITIES
16 Base facilities (including shelters, power generation, water supplies)
17 Expedient roads/airfields/bridges
18 Amphibious operations (including breakwaters, wave forces)
19 Over-the-Beach operations (including containerization, material transfer, lighterage and cranes)
20 POL storage, transfer and distribution

28 ENERGY/POWER GENERATION
29 Thermal conservation (thermal engineering of buildings, HVAC systems, energy loss measurement, power generation)
30 Controls and electrical conservation (electrical systems, energy monitoring and control systems)
31 Fuel flexibility (liquid fuels, coal utilization, energy from solid waste)
32 Alternate energy source (geothermal power, photovoltaic power systems, solar systems, wind systems, energy storage systems)
33 Site data and systems integration (energy resource data, energy consumption data, integrating energy systems)
34 ENVIRONMENTAL PROTECTION
35 Hazardous waste minimization
36 Restoration of installations (hazardous waste)
37 Waste water management and sanitary engineering
38 Oil pollution removal and recovery
39 Air pollution

44 OCEAN ENGINEERING
45 Seafloor soils and foundations
46 Seafloor construction systems and operations (including diver and manipulator tools)
47 Undersea structures and materials
48 Anchors and moorings
49 Undersea power systems, electromechanical cables, and connectors
50 Pressure vessel facilities
51 Physical environment (including site surveying)
52 Ocean-based concrete structures
54 Undersea cable dynamics

TYPES OF DOCUMENTS

85 Techdata Sheets 86 Technical Reports and Technical Notes
83 Table of Contents & Index to TDS
82 NCEL Guides & Abstracts
91 Physical Security

☐ None-remove my name

NCEL DOCUMENT EVALUATION

You are number one with us; how do we rate with you?

We at NCEL want to provide you our customer the best possible reports but we need your help. Therefore, I ask you to please take the time from your busy schedule to fill out this questionnaire. Your response will assist us in providing the best reports possible for our users. I wish to thank you in advance for your assistance. I assure you that the information you provide will help us to be more responsive to your future needs.

R. N. STORER, Ph.D, P.E.
Technical Director

DOCUMENT NO. _____ TITLE OF DOCUMENT: _____

_____

Date: _____ Respondent Organization : _____

Name: _____ Activity Code: _____
Phone: _____ Grade/Rank: _____

Category (*please check*):

Sponsor ____ User ____ Proponent ____ Other (*Specify*) _____

Please answer on your behalf only; not on your organization's. Please check (*use an X*) only the block that most closely describes your attitude or feeling toward that statement:

SA Strongly Agree **A** Agree **O** Neutral **D** Disagree **SD** Strongly Disagree

---

		SA	A	N	D	SD
1.	The technical quality of the report is comparable to most of my other sources of technical information.	( )	( )	( )	( )	( )
2.	The report will make significant improvements in the cost and or performance of my operation.	( )	( )	( )	( )	( )
3.	The report acknowledges related work accomplished by others.	( )	( )	( )	( )	( )
4.	The report is well formatted.	( )	( )	( )	( )	( )
5.	The report is clearly written.	( )	( )	( )	( )	( )
6.	The conclusions and recommendations are clear and directly supported by the contents of the report.	( )	( )	( )	( )	( )
7.	The graphics, tables, and photographs are well done.	( )	( )	( )	( )	( )

Do you wish to continue getting NCEL reports? ☐ YES ☐ NO

Please add any comments (e.g., in what ways can we improve the quality of our reports?) on the back of this form.

Comments:

Please fold on line and staple

DEPARTMENT OF THE NAVY

Naval Civil Engineering Laboratory
Port Hueneme, CA 93043-5003

Official Business
Penalty for Private Use $300

Code L03B
NAVAL CIVIL ENGINEERING LABORATORY
PORT HUENEME, CA 93043-5003